https://doi.org/10.5194/egusphere-2026-1699
Preprint. Discussion started: 13 April 2026

Disentangling the contributions of external forcings and internal factors to future alpine sediment fan dynamics

Philipp D. Gewalt[1], Thomas C. Wagner[2], Michael Krautblatter[1]

[1]Chair of Landslide Research, Technical University of Munich, Germany
[2]Chair of Restoration Ecology, Technical University of Munich, Germany

Correspondence to: Philipp D. Gewalt (philipp.gewalt@tum.de)

Abstract. Alpine alluvial fans and debris flow cones are central components of mountainous sediment cascades. The projected increase in heavy precipitation due to ongoing climate warming has been shown to intensify sediment redistribution dynamics under transport-limited conditions; however, sediment fan response to heavy precipitation has been shown to be strongly system-specific. The relative importance of external forcings and internal factors for sediment dynamics and their implications for sediment fan evolution in a future changing climate have not been assessed systematically so far. In this study, we compare decadal-scale planimetric dynamics of a mature alpine alluvial fan ("Friedergries", 5 km^2 catchment area) to juvenile debris flow cones (Lake Plansee, catchment areas mostly < 0.5 km^2) in the Main Dolomite region of the Northern Calcareous Alps. In both areas, planimetric sediment redistribution dynamics are governed by external forcing by heavy rainfall. Internal system variables such as catchment morphometry transform the external forcing: the juvenile cones corresponding to small and steep catchments are susceptible to moderate precipitation extremes (< 1 year return interval) while floodplain dynamics on the mature fan are only susceptible to extreme precipitation events with supra-regional extent (3–20 years return interval). A detailed analysis of volumetric changes at Friedergries from 2018 to 2024 reveals that total erosion and deposition are best explained by heavy precipitation, while the location and timing of incision and backfill are determined by small-scale autogenic cycles. Based on current projections of climate change in the European Alps, we suggest that future sediment fan dynamics will be characterized by (i) an intensification of sediment redistribution in response to rainfall intensification, (ii) an increase of geomorphic work per rainstorm event in response to rainfall concentration, (iii) an increase in likelihood of system state changes, and (iv) a catchment-dependent seasonal shift of sediment redistribution: Activity of juvenile cones with small, steep catchments will shift towards spring and autumn while mature fans with larger, gentler catchments will continue to experience sediment redistribution mainly in summer. Here we show that catchment morphology and fan maturity control future susceptibility to rainstorms and thus sediment fan evolution in the coming decades.

https://doi.org/10.5194/egusphere-2026-1699
Preprint. Discussion started: 13 April 2026

1 Introduction

Alpine alluvial fans and debris flow cones are important sediment storages in mountain cascades (Franke et al., 2015; Harvey, 2010), important settlement space (Chiverell & Jakob, 2013; Fischer, 1966; Turkington et al., 2016; Hock et al., 2019), act as a hydrologic buffer (Herron & Wilson, 2001; Hayashi, 2020) and provide habitats for rare specialist species (Wöllner & Wagner, 2019; Wagner & Zehm, 2022). Sediment redistribution on alpine alluvial fans and debris flow cones (hereafter collectively referred to as "alpine sediment fans", Franke et al., 2015) is determined by external forcings and internal factors, including feedbacks and thresholds (Milan, 2021; Scott & Erskine, 1994). The dominant external forcing in the European Alps is heavy precipitation, as the two main processes reworking alpine sediment fans, fluvial discharge and debris flows, are both strongly dependent on heavy precipitation (Caine, 1980; Guzetti et al., 2008; Kaitna et al., 2013; Milan & Schwendel, 2021; Brunner et al., 2021). Ongoing climate warming alters precipitation regimes in the European Alps: until the end of the 21st century, extreme precipitation events are projected to increase across all seasons (Gobiet et al., 2014; Estermann et al., 2025; Kotlarski et al., 2023), leading to higher discharges especially in high elevation catchments (> 1000 m a.s.l.; Brunner et al., 2021). Changing precipitation regimes will likely impact sediment dynamics on alpine sediment fans: For debris flows, Turkington et al. (2016) report an increase in heavy precipitation events potentially triggering debris flows until the end of the 21st century. Kiefer, Oswald et al. (2021) relate a seven-fold increase in debris flow activity in the Northern Calcareous Alps after the 20th century to a two-fold increase in heavy precipitation events. Stoffel et al. (2014) and Kaitna et al. (2023) postulate a shift of debris flow activity towards spring and autumn. For fluvial systems, numerical modelling and geomorphic theory suggest increases of catchment sediment yield, bank erosion, higher magnitude scour-and-fill-cycles, and planform changes in response to higher discharges and potentially higher sediment input from the hillslopes (East & Sankey, 2020; East et al., 2017). Coupling a climate model and a sediment transport model, Kido et al. (2023) predict that sediment yield from a Japanese mountain stream will increase by a factor of 3–5.5 in response to an increase of short-term heavy precipitation. Praskievicz (2015) predicts future sediment dynamics of three mountain streams based on projections of future discharges, showing either increases or decreases of bedload transport depending on increasing/decreasing durations of critical shear stress exceedance. However, observational studies yield ambiguous results, with climatic forcing only partly explaining temporal variability of sediment yield and morphological changes (East & Sankey, 2020). This is due to the fact that a given fan system's response to a heavy precipitation event is strongly influenced by internal factors such as sediment availability (Hirschberg et al., 2021; Jomelli et al., 2007), fan and channel morphology (Scott & Erskine, 1994; Wells & Harvey, 1987; Bakker et al., 2019; Milan & Schwendel, 2021), sediment erodibility and location of sediment storages, and resulting thresholds for bedload mobilization and transport (Milan, 2021). These internal factors are modified by extreme events, whose influence can persist for several years to decades (East & Sankey, 2020; Harvey, 2007; Milan & Schwendel, 2021; Rainato et al., 2025). For meaningful inferences about future sediment fan dynamics, it is necessary to disentangle the relative importance of external forcings and internal feedbacks and thresholds. Measuring the impact of climatic forcing on geomorphic processes is best possible in regions with high geomorphic process rates and transport-limited conditions ("sentinel regions", East & Sankey, 2020). The dolomitic

https://doi.org/10.5194/egusphere-2026-1699
Preprint. Discussion started: 13 April 2026

regions of the Northern Calcareous Alps satisfy both conditions, showing high geomorphic process rates (Kiefer, Oswald et al., 2021; Götz & Schrott, 2025), extensive storages of loose debris, and high weathering rates (Bayerisches Geologisches Landesamt, 1996; Sass, 2005) in addition to the highest projected changes in heavy precipitation in the European Alps (Rajczak et al., 2013). To investigate the relative importance of external climatic forcing and internal feedbacks and thresholds in this region we aim to

(i) Derive a sediment redistribution chronology for an active "model" sediment fan
(ii) Quantify climatic forcing of sediment redistribution
(iii) Detect and quantify system thresholds and autogenic behaviour
(iv) Decipher how catchment morphology and fan maturity shape future sediment fan dynamics in a changing climate.

2 Study areas

The Friedergries is located in the Northern Calcareous Alps about 10 km west of Garmisch-Partenkirchen (47° 29' 25'' N, 10° 57' 03'' E; Figure 1). It is the mature alluvial fan of the alpine stream Friederlaine. The Friedergries has an area of 0.9 km^2 and forms a near-perfect cone with a slope of about 5 % (Figure 2). The uppermost 300 m downstream of the fan apex are characterized by a well-developed fanhead trench bordered by a terrace staircase, its inflection point is about 500 m downstream of the fan apex.

Runoff at the Friederlaine is high during snowmelt in early summer and reacts rapidly to heavy precipitation during thunderstorms. During dry periods, the Friederlaine infiltrates into the permeable gravel. The water continues as sub-surface flow and resurfaces in the lower southwestern part of the fan. Thus, the upper and lower part of the fan are disconnected in terms of bedload transport during stages of low flow. A pilot study found a total of 4400 m^3 of erosion between October 2016 and 2017 in the uppermost 200 m from the fan apex (Wöllner & Wagner, 2019).

The Friederlaine catchment has an area of 5 km^2 with a mean elevation of 1536 m a.s.l. (930 to 2080 m a.s.l). Historical topographic maps show that the main channel of the Friederlaine and thus the area of sediment redistribution were situated in the eastern sector of the fan from at least 1826 to 1920 (LDBV, 1826, 1835, 1880, 1912, 1923). Reports from the 1920s/1930s describe the onset of channel migration towards the central part of the fan (Doposcheg, 1938; Koegel, 1920). Starting in the 1930s, dams were constructed to confine the Friederlaine to its eastern course (Doposcheg, 1938). The largest of these dams ("Franzosenmauer") was constructed during World War II, possibly in response to a regional rainfall event in 1940 (Fischer & Stängl, 1941), and consisted of a high dam and a bypass channel at the fan apex. It broke in the 1960s. While the exact timing of the dambreak remains uncertain, it is probable that happened contemporaneously to the 1965 Danube Whitsuntide flood (Kern & Streil, 1972).

https://doi.org/10.5194/egusphere-2026-1699
Preprint. Discussion started: 13 April 2026

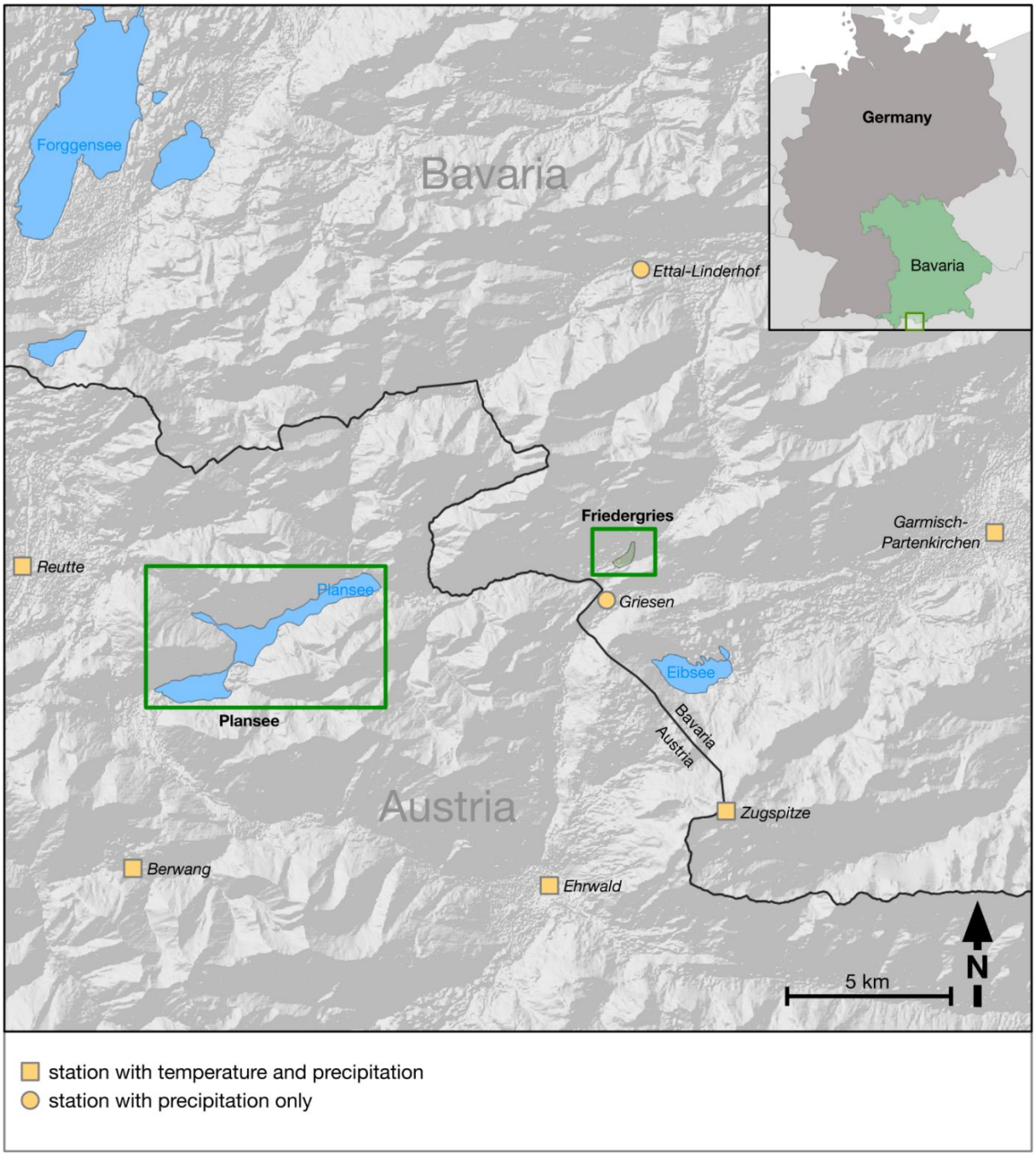

Figure 1: Overview map of the main study site (Friedergries), the reference site (Plansee), and the location of the climate stations. Basemap data sources: openstreetmap.org and contributors, Copernicus WorldDEM-30 © DLR e.V. 2010-2014 and © Airbus Defence and Space GmbH 2014-2018 provided under COPERNICUS by the European Union and ESA; all rights reserved. Data available at https://doi.org/10.5270/ESA-c5d3d65).

https://doi.org/10.5194/egusphere-2026-1699
Preprint. Discussion started: 13 April 2026

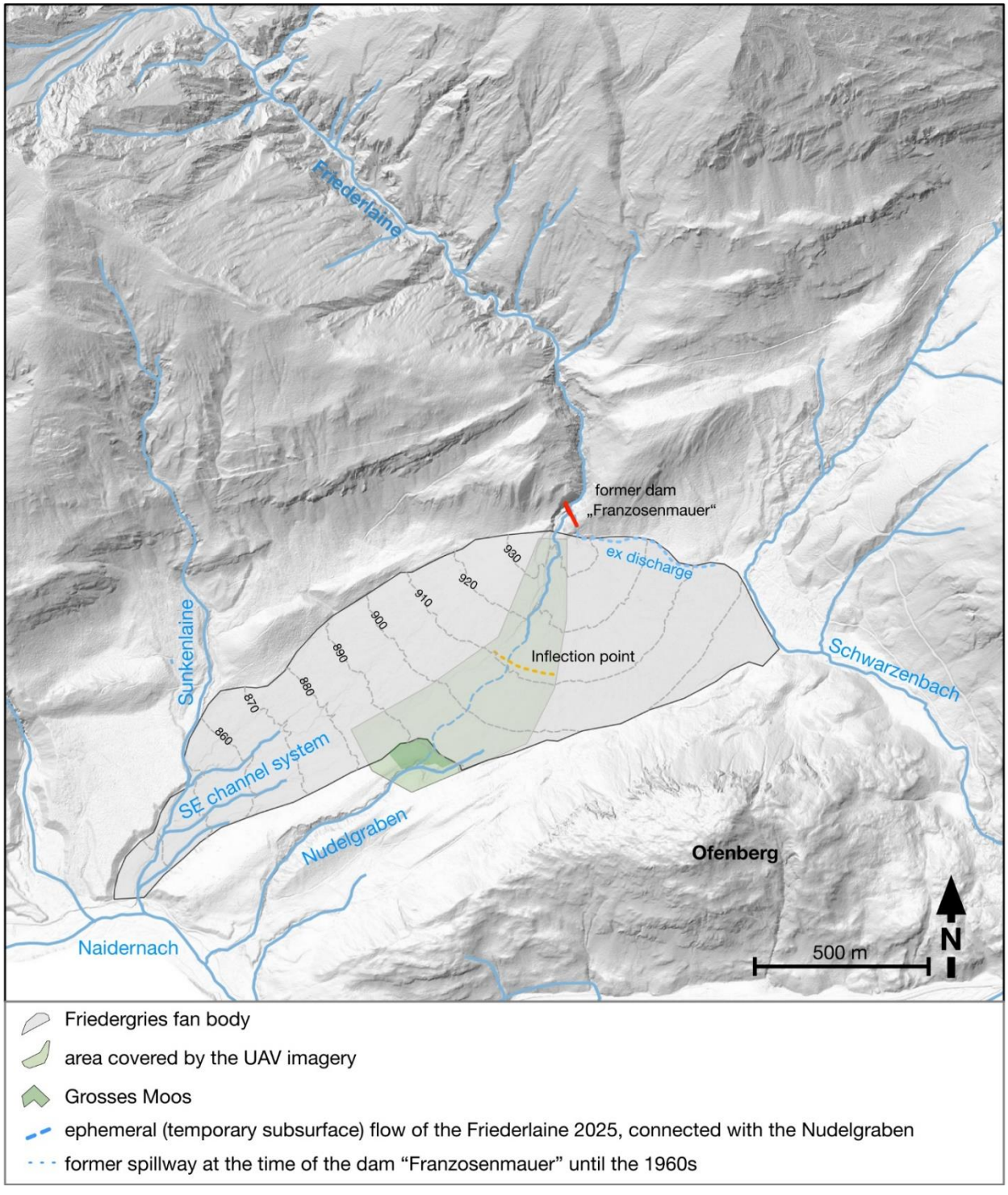

Figure 2: Detail map of the study site (Friedergries) with its main drainage system. Basemap data source: Bayerische Vermessungsverwaltung (BVV), BayernAtlas / GeodatenOnline – www.geodaten.bayern.de

https://doi.org/10.5194/egusphere-2026-1699
Preprint. Discussion started: 13 April 2026

To provide regional context for our investigation at Friedergries, we compare our results to existing data from Lake Plansee (Kiefer, Oswald et al., 2021; Barbosa, Kiefer et al., in prep.). The Plansee catchment is located about 10 km west of Friedergries. Lake Plansee is bordered by numerous, mostly juvenile debris flow fans, alluvial fans, and fan deltas (Kiefer, Oswald et al., 2021). Similar to Friedergries, the mean elevation of their catchments is 1519 m a.s.l. (980 to 2250 m a.s.l.). For this study, we use decadal data from Barbosa, Kiefer et al. (in prep.) who report the aggregated active area of 60 fans. As some fans have secondary feeder channels in addition to the main feeder channel, we investigate the morphology of 69 sub-catchments.

Both Friedergries and Plansee are situated in the Main Dolomite (local name: Hauptdolomit) region of the Northern Calcareous Alps. Main Dolomite is an intensely jointed Triassic dolostone with a wide extent, forming numerous peaks in the Northern Calcareous Alps. It is highly conducive to physical weathering and rockfall and a major source of loose debris (Sass, 2005; Bayerisches Geologisches Landesamt, 1996). Therefore, rapid sediment recharge of stream channels can be expected after sediment export events, implying transport-limited conditions for both Friedergries and Plansee.

During our study period, several major heavy rain events occurred in the wider region. In 1965, a Vb event led to widespread floodings in Austria and Bavaria (Kern & Streil, 1972; Hydrographischer Dienst Österreich, 1970; Stahl & Hofstätter, 2018), with extremely high discharges registered at the Loisach gauge at Garmisch-Partenkirchen. In 1977 and 1981, heavy precipitation events along the Northern Alps caused widespread floods, debris flows, and slope movements throughout Austria and eastern Switzerland (Hydrographischer Dienst Österreich, 1981, 1984; Zeller & Röthlisberger, 1984; Gerig, 1977; Kälin, 1977; Gruber, 1977). In 2002, a Vb event led to several floods in the Alpine region (Weber & Braun, 2014). In 1999 and 2005, two extreme heavy rain events occurred, causing damages in northeastern Switzerland, western Austria and southern Bavaria as well as widespread fluvial sediment redistribution, debris flows, and landslides (Weber & Braun, 2014; Bezzola & Hegg, 2007; Godina et al., 2006; LfU, 2007; Rickenmann & Koschni, 2010; Aschwanden, 2000; Landesamt für Wasserwirtschaft, 2003). At the nearby Loisach gauge these rain events led to the highest (1999) and second highest (2005) discharges measured since the start of measurements in November 1962 (GWKD, 2021). In the neighbouring Wetterstein mountains, the August 2005 flood profoundly altered the morphology of the Partnach River headwaters (Morche et al., 2006). In 2024, a heavy precipitation event with a duration of several days affected southern Bavaria and adjacent regions (LfU, 2025).

3 Material and methods

3.1 Pre-existing geodetic datasets and historical imagery

For Friedergries, we acquired pre-existing orthophotos, digital elevation models (DEMs), and digital surface models (DSMs) from the Bavarian mapping authorities (LDBV). For 2024, we downloaded the orthophoto and DSM derived from aerial imagery. For 2019, we downloaded aerial LiDAR derived elevation data both as a DEM of 1 m cell size and as point cloud

https://doi.org/10.5194/egusphere-2026-1699
Preprint. Discussion started: 13 April 2026

data (LDBV, 2025). We used the point cloud to derive a DSM of 40 cm cell size that was aligned to the 2022 40 cm orthophoto. For Plansee, we acquired the 0.5 m resolution DEM from 2019 (Land Tirol, 2025). For the timeframe 1945–2022, we acquired historical aerial imagery from the Austrian and Bavarian mapping authorities. Starting in 2009, the aerial imagery was acquired in a digital format, prior to 2009 we received both high-resolution scans of the original films and low-resolution scans of paper copies of the imagery (Supplement 1). We obtained active area data for Plansee from Barbosa, Kiefer et al. (in preparation).

3.2 Data preparation

3.2.1 Historical aerial imagery: orthomosaic generation

Aerial imagery was processed with Agisoft Metashape v1.6.2. We manually marked fiducial marks and calibrated the fiducials with the inbuilt routine and information on scanning resolution. Due to the well-defined geometry of survey-grade cameras, we used a simple camera model with principal point offset (cx, cy), focal distance (f), and three radial distortion parameters (k1, k2, k3) (Agisoft, 2025). When camera calibration reports were available (20 of 25 flight campaigns; Supplement 1), we calculated model parameters from the reports and fixed them during image alignment. Otherwise, we performed self-calibration. We identified ground control points we could reasonably assume to be stable, e.g. building roofs, crossroads, and ground points between conspicuous groups of trees and bushes and derived their x, y, z-coordinates from the 2022 orthophoto and the 2019 DSM. We performed an initial image alignment either based on camera positions (if available) or 3-4 ground control points to establish an image network. After the initial alignment, we placed additional ground control points (GCPs) and check points (CPs), reset the alignment, and performed a second alignment. We checked GCP and CP residuals, investigated the source of high residuals and adjusted or deleted GCPs and CPs wherever necessary before performing a final alignment. Finally, we calculated a dense point cloud, DSM, and an orthomosaic. If image alignment was achieved but point cloud quality or extent were insufficient to generate reliable DSMs, we projected the images on the 2019 LiDAR DEM for orthomosaic generation. For 1947 (1 image) and 1969 (2 images), no image alignment could be achieved. We georeferenced these images to the 2022 orthophoto using an affine transformation in ArcGIS Pro 3.1.0.

3.2.2 UAV-based sub-annual geomorphic change detections

Between June 2018 and October 2024, seventeen drone flights with a commercial DJI P4P drone equipped with a standard RGB camera were carried out. Mission planning was done with MapPilot Pro, using standard missions with a flight height of 40 m above ground level and an image overlap of 80 % at a speed of 4 m s^{-1}. The acquired images were processed using Agisoft Metashape Pro 2 to create a point cloud, digital surface model, and orthomosaics (Agisoft, 2025). Ground points were identified using a max angle of 10°, a maximum distance of 0.1 m, an assumed max. terrain slope of 90° and a cell size of 10 m. The erosion radius was set to 0.02 m. The resulting ground points were manually cleaned of outliers and used to create a digital elevation model (DEM) without vegetation. The quality and resolution of the images varied slightly between flights depending on light and weather conditions. Orthoimages achieved a resolution of 1.5–2 cm px^{-1}, DSMs achieved an x-y-

https://doi.org/10.5194/egusphere-2026-1699
Preprint. Discussion started: 13 April 2026

resolution of 3–4 cm px^{-1} and a vertical resolution of 4–5 cm px^{-1}. For horizontal alignment, orthoimages, DSMs, and DEMs were co-registered to the official 2022 orthoimage. To achieve vertical alignment, DSMs and DEMs were referenced to the 40 cm LiDAR DSM from 2019. To correct for non-linear distortions such as the doming effect typical of photogrammetric DSMs (James & Robson, 2014), we used a reference surface approximating the spatially variable height offset (Wöllner & Wagner, 2019): Based on the aerial photographs, 96 stable ground points (points that were not subject to any real change in height) were selected across the study area. For each reference point, the "true" altitude based on the 2019 lidar data and the altitude according to the DEM of the respective flight were sampled and subtracted from each other. We interpolated these height differences linearly and subtracted them from the DSMs and DEMs. The quality of the alignment was checked by comparison of elevation profiles in stable areas of the study region. The co-registered DEMs were used to create DEMs of difference (DoD) for change detection between consecutive flights. This resulted in 16 change detection epochs, ten of which are short (< 100 d) summer epochs and six of which are long (> 250 d) winter epochs (Table A1). We manually delineated the area of interest for geomorphic change detection from inspection of consecutive hillshades. To investigate spatial patterns of change, we divided the area of interest into nine concentric rings of 100 m width centred at the fan apex.

We estimated DoD uncertainty with the method of Anderson (2019). It partitions the uncertainty into systematic, spatially correlated, and spatially uncorrelated random uncertainty. We estimated the uncertainty on the DoD of a calibration area that remained unchanged throughout the whole survey time. We subsampled the DoD to 1 m resolution and estimated systematic uncertainty as the absolute mean bias error (MBE) and random uncertainty as the standard deviation (STD) of the DoD in the calibration area. To constrain spatially correlated uncertainty, we fitted a spherical semivariogram model to the DoD of the calibration area with the ArcGIS Pro Geostatistical Wizard. Since the empirical semivariogram could not be fitted well with a semivariogram model without a nugget as proposed by Anderson (2019), we used the method of Rolstad et al. (2009) to calculate spatially correlated error. We did not perform trend removal (Gringarten & Deutsch, 2001; Burrough & McDonald, 1998), assuming that large-scale trends had already been removed during vertical alignment. To calculate net change for the whole timespan, we summed the net changes of all timespans. We applied error propagation with correlated variables (Vermeesch, 2017; Ku, 1966; Dodge, 2008; Appendix D).

3.2.3 Weather data

Neither the Friedergries catchment nor the Plansee catchment have a weather station. Therefore, we acquired weather data for seven weather stations in the vicinity of the catchments (Figure 1, Table 1).

https://doi.org/10.5194/egusphere-2026-1699
Preprint. Discussion started: 13 April 2026

Table 1: Metadata of weather stations used in this study.

Name	Abbreviation	Lon (°)	Lat (°)	Data type	Temporal Resolution	Timeframe	Source
Ettal-Linderhof	ELI	10.956	47.570	precipitation	1 d	01.01.1961-31.12.2024	GKD (2025)
Griesen (801 m a.s.l.)	GRI	10.944	47.478	precipitation	1 d, 5 min	08.04.2004-31.12.2024	GKD (2025)
Reutte (850 m a.s.l.)	REU	10.715	47.494	precipitation, temperature	1 d	01.01.1936-31.12.2024	Geosphere Austria (2025)
Garmisch-Partenkirchen (720 m a.s.l.)	GAP	11.062	47.483	precipitation, temperature	1 d	01.01.1936-31.12.2024	DWD (2025)
Zugspitze (2956 m a.s.l.)	ZUG	10.985	47.421	precipitation, temperature	1 d	01.08.1900-31.12.2024 (temperature) 31.12.1900-31.12.2024 (precipitation)	DWD (2025)
Berwang (1295 m a.s.l.)	BER	10.751	47.408	precipitation, temperature	1 d	01.01.1998-31.12.2022 (temperature) 01.08.1895-31.12.2022 (precipitation)	BMLUK (2025)
Ehrwald (1000 m a.s.l.)	EHR	10.920	47.404	precipitation, temperature	1 d	01.08.1972-31.12.2024	Geosphere Austria (2025)

To estimate the mean daily air temperature at Friedergries and Plansee, we use data from Reutte, Berwang, Ehrwald, Zugspitze, and Garmisch-Partenkirchen. From their mean annual air temperatures, we calculate the regional temperature lapse rate as –5.49 °C/km. We calculate the mean daily air temperature at the respective mean catchment heights by applying this lapse rate and inverse distance weighted interpolation (Achilleos, 2011).

https://doi.org/10.5194/egusphere-2026-1699
Preprint. Discussion started: 13 April 2026

3.3 Data analysis

All GIS analyses were carried out in ArcGIS Pro (version 3.1.0) and QGIS (version 3.42). Data analysis was carried out with Python 3.8.10, with the modules numpy (version 1.24.2; Harris et al., 2020) and scipy (version 1.10.1; Virtanen et al., 2022).

3.3.1 Morphological catchment analysis

To provide background information for geomorphic change detections and climate data analysis, we perform morphometric analyses on the Plansee and Friedergries catchments. For both sites, the analysis is based on the respective 2019 DEM. We describe each catchment by four metrics: catchment area, catchment circularity, maximum flow length, and mean channel slope. We use standard hydrological workflows to delineate catchments. Based on the catchments, we derive the stream network. We assume that channelized flow starts when the contributing drainage area exceeds 10 000 m^2. As a measure of channel slope, we calculate the mean slope along the longest channelized flow path.

3.3.2 Constraining historical active area/decadal sediment dynamics

The quality of the older DSMs was insufficient for geomorphic change detection as elevation changes on the fan mostly range from a few decimeters to 2 m, which is in the same order of magnitude as the uncertainty of DSM reconstruction from the historical imagery. Therefore, we adopted active area as a proxy for sediment redistribution. We define active area as the area experiencing reworking by geomorphic processes. Increases of active area are due to the deposition of fresh, lightly coloured sediments in previously weathered and/or vegetated areas as well as the erosion of weathered surface sediments, exposing the fresh and lightly coloured underlying sediments. This is immediately visible in aerial imagery. In contrast, decreases in active area are not immediately visible as the darkening of the surface sediments takes time. For the main lithology of the Friedergries debris, Main Dolomite, this weathering timespan is estimated as five years (Friedel, 1935). Active area increases during discharge events of a magnitude exceeding the capacity of the previously active channel and floodplain. Consequently, a chronology of active area reflects extreme events. However, the threshold above which a discharge event is considered an extreme event will differ between different sediment fans, as the fan system response to a discharge event depends on characteristics of the fan (Scott & Erskine, 1994; Lane & Richards, 1996) and catchment (Liebscher, 1996; Legarda Garzon et al., 2023; Milan, 2021). We assume that active area can serve as a semi-quantitative measure of sediment redistribution intensity when (i) active area is not constrained (e.g. by bedrock outcrops) and (ii) fluvial channels are shallow and narrow and can relocate in response to sediment redistribution. These are satisfied as (i) the active area was located in the central part of the fan for the whole period of our investigation and (ii) both high-resolution UAV surveys and in-person fieldtrips confirm multiple avulsions of small channels downstream of the fanhead trench since 2018. We manually digitize active area from the historical orthophotos. In addition to the colour of the sediments, we check for signs of sediment redistribution during the delineation of active area (e.g. changes to fluvial channels, erosion along terraces, deposition lobes). To limit bias, this step was completed by the same worker for all timeframes.

https://doi.org/10.5194/egusphere-2026-1699
Preprint. Discussion started: 13 April 2026

3.3.3 Estimating sediment storage behind the Franzosenmauer dam

We estimate sediment storage upstream of the Franzosenmauer dam based on the DEM from 2019 and the orthophoto of 1960. The 1960 orthophoto shows that the accommodation space upstream of the Franzosenmauer dam was completely filled with sediment. We use the lowest point of the artificial bypass channel at 950 m a.s.l. as an estimate for the minimum height of the Franzosenmauer dam. We use the extent of the dam determined from the 1960 orthophoto in conjunction with the 2019 DEM to model the Franzosenmauer dam as a triangular prism. We model the sediment storage upstream of the Franzosenmauer dam as a floodplain sloping gently to the south. To obtain a lower and upper bound estimate of the stored sediment volume, we assume a floodplain inclination of 2 % and 7 %, respectively. For each of these cases, we produce altered versions of the 2019 DEM and perform geomorphic change detections between the artificial DEMs and the true DEM to estimate the volume of the stored sediment.

3.3.4 Statistical modelling

The ultimate aim of climate data analysis was to investigate links between geomorphic change and weather data. We define four different precipitation statistics (Table 2).

Table 2: Definition of precipitation statistics.

Statistic	Unit	Definition	Mathematical formulation	Eq.
Total precipitation	mm	Total sum of precipitation.	$\sum_{i=1}^{n} p_i$	(1)
Total liquid precipitation	mm	Sum of precipitation on days with mean daily air temperature > 0°C.	$\sum_{i=1}^{n} f(p_i, T_i)$ $f(p_i, T_i, t) = \begin{cases} p_i \; for \; T_i > 0°C \\ 0 \; for \; T_i \leq 0°C \end{cases}$	(2)
Precipitation sum above a threshold	mm	Sum of precipitation exceeding an intensity threshold (Ariagno et al., 2022).	$\sum_{i=1}^{n} g(p_i, t)$ $g(p_i, t) = \begin{cases} p_i - t \; for \; p_i > t \\ 0 \; for \; p_i \leq t \end{cases}$	(3)
Liquid precipitation sum above a threshold	mm	Sum of precipitation exceeding a threshold on days with mean daily air temperature > 0°C.	$\sum_{i=1}^{n} h(p_i, T_i, t)$ $h(p_i, T_i, t) = \begin{cases} p_i - t \; for \; p_i > t \; and \; T_i > 0°C \\ 0 \; for \; p_i \leq t \; or \; T_i \leq 0°C \end{cases}$	(4)

https://doi.org/10.5194/egusphere-2026-1699
Preprint. Discussion started: 13 April 2026

p_i : precipitation sum of the ith datapoint (mm d^{-1}); t: threshold (mm d^{-1}); T_i: interpolated mean daily temperature at Friedergries/Plansee for the ith datapoint (°C)

The definition of these precipitation statistics is based on the following rationales: snow and rain behave fundamentally different in terms of runoff and sediment redistribution. While heavy rainfall generates runoff immediately, heavy snowfall is stored until melt (Brunner et al., 2021). However, snowmelt can be a substantial contributor to runoff and sediment transport in spring (Rainato et al., 2025; van Hamel et al., 2025; Lana-Renault et al., 2011). Therefore, we analyze the link between liquid precipitation and sediment redistribution and total precipitation (including rain and snow) and sediment redistribution separately.

Models based on precipitation above a threshold reflect the observation that sediment redistribution starts above a precipitation threshold (Ariagno et al., 2022). Peak flow generated during a given precipitation event depends on catchment characteristics (Liebscher, 1996; Legarda Garzon et al., 2023). Therefore, the threshold cannot be known a priori and needs to be calibrated. To achieve calibration, we calculate linear models for a range of thresholds and choose the best performing model based on R^2 (cf. Ariagno et al., 2022).

For model construction, we adopted different approaches for the temporally and spatially highly resolved sub-annual UAV-DSMs and the long term decadal orthophotos.

For the UAV change detection, we based our analysis on the precipitation data from Griesen. We calculated precipitation statistics for each change detection epoch. We then performed separate ordinary least squares linear regression analyses of total erosion and total deposition on the precipitation statistics (Table 2). We calculated regressions for two scenarios: in the first scenario ("all data"), we included data from all epochs, in the second scenario ("net negative"), we excluded all epochs with net deposition, i.e. epochs in which we can be sure of significant sediment input from the catchment. For the regressions for deposition, we excluded epoch 14 because of considerable sediment export from our area of investigation.

For the aerial imagery, we based our analysis on daily precipitation data from all weather stations used in this study. Based on our assumption about the weathering timespan necessary to visibly darken the sediments in the aerial imagery, we calculated precipitation statistics for five-year periods preceding each flight campaign for each station separately (e.g. for the flight campaign on 09.10.1969 we calculated precipitation statistics for the period 09.10.1962–08.10.1969; cf. East et al., 2017). The statistics were only calculated for periods without data gaps (WMO, 2017). To derive the regional trend, we averaged the statistics of all seven weather stations. We only calculated averages if data from at least three stations were available, else we eliminated the 5-year period from the analysis. To assess the influence of the choice of the weathering timespan on our results, we conduct a sensitivity analysis with weathering timespans of 4, 5, and 6 years (Appendix E). To quantify the importance of regional heavy precipitation, we calculate the contribution of the heavy rain events listed in Sect. 2 to 5-year precipitation statistics.

In addition to the precipitation statistics in Table 2, we calculated 1-day return intervals with the partial series method (DWA, 2012) for the timeframe 1973–2022 for which all stations have precipitation data (Appendix C). We did not apply the moving

https://doi.org/10.5194/egusphere-2026-1699
Preprint. Discussion started: 13 April 2026

window correction, thus our return intervals represent daily return intervals, not 24 h return intervals. For Griesen, the calculation of return intervals was not feasible as the record is too short.

We excluded some datapoints from the calculation of linear models: At Friedergries, we exclude data points prior to 1977 due to incomplete sediment storage exhaustion behind the Franzosenmauer. We exclude 2024 because of insufficient precipitation data coverage (only two weather stations provide complete precipitation chronologies) and the formation of a continuous central channel that channels runoff and thus impedes overbank flow and areal sediment reworking (cf. assumption (ii) from Sect. 3.3.2). At Plansee, we exclude 1952 as a conspicuous outlier.

4 Results

4.1 Catchment morphologies at Friedergries and Plansee

Catchments at Plansee are generally smaller, have much shorter maximum flow lengths, and higher mean channel slopes compared to the Friederlaine catchment (Figure 3, Supplement 2). Median catchment areas at Plansee are 7.9 ha, median maximum flow length is 480 m, and median mean channel slope is 32.5° compared to 500 ha (6300 %), 4850 m (1000 %), and 11.7° (36 %) at Friedergries. Visual inspection of the hillshades shows that the assumed start of channelized flow below a contributing drainage area of 10 000 m^2 seems to coincide reasonably well with the location of couloirs, gullies, and fluvial channels.

https://doi.org/10.5194/egusphere-2026-1699
Preprint. Discussion started: 13 April 2026

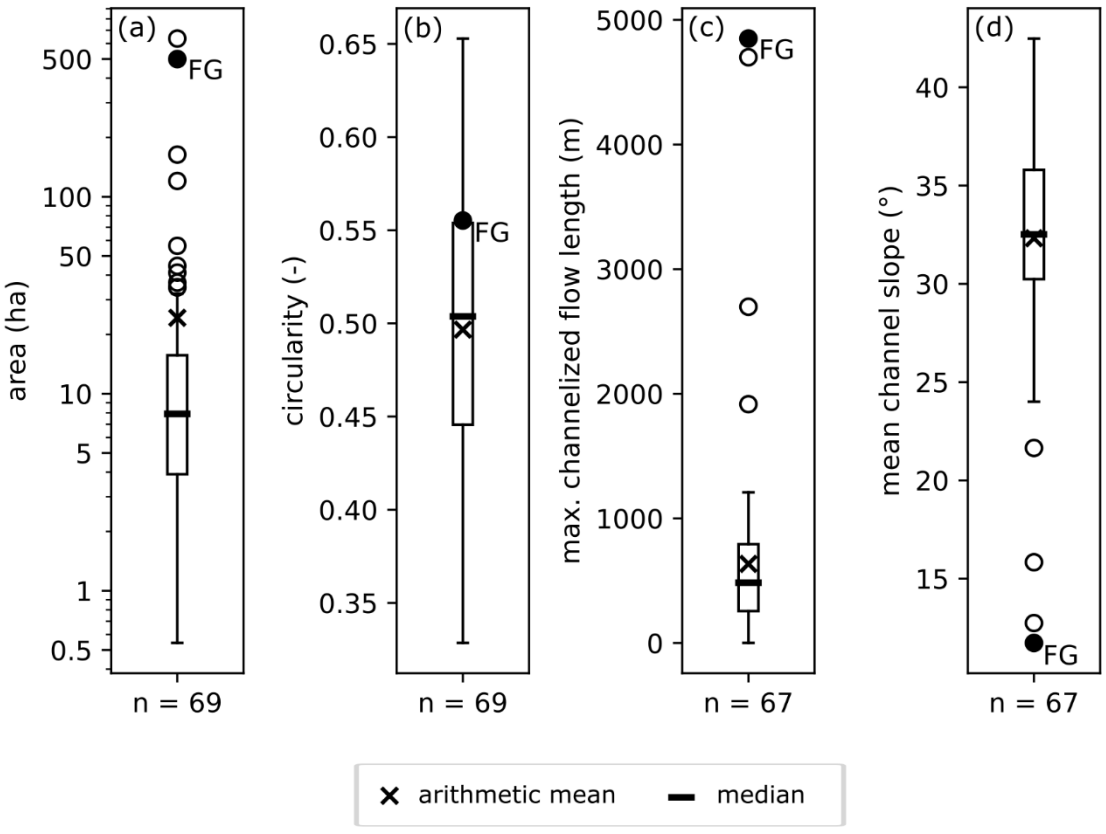

Figure 3: Summary of the morphological analysis of the Plansee and Friedergries catchments. (a): area (note logarithmic y-scale), (b): circularity, (c): maximum channelized flow length, (d): mean slope. For the full list of catchment properties, see Supplement 2.

4.2 Decadal sediment redistribution

4.2.1 Floodplain migration and channel avulsion

Decadal geomorphological dynamics at Friedergries are characterized by gradual floodplain migration disrupted by one major avulsion following the breaking of the Franzosenmauer dam. Active area expanded and shrunk periodically with minima in 1952, 1969, the late 1980s, and since 2015, and maxima in 1966, 1983, and the early 2000s (Figure 5).

From 1945 to 1966, the main course of the Friederlaine was forced southeast by the Franzosenmauer dam. However, an active area in the central sector of the fan attests to spillover events with associated sediment reworking. Between 1960 and 1966, the Franzosenmauer dam broke. Strong incision resulted in the formation of terrace staircases on both the northeastern and the central floodplain that are still visible today. The dambreak led to the inactivation of the northeastern floodplain and the release

https://doi.org/10.5194/egusphere-2026-1699
Preprint. Discussion started: 13 April 2026

of 24000–36000 m^3 of sediment previously stored upstream of the Franzosenmauer dam. However, historical orthophotos show that the release of sediment wasn´t completed until the mid-1970s.

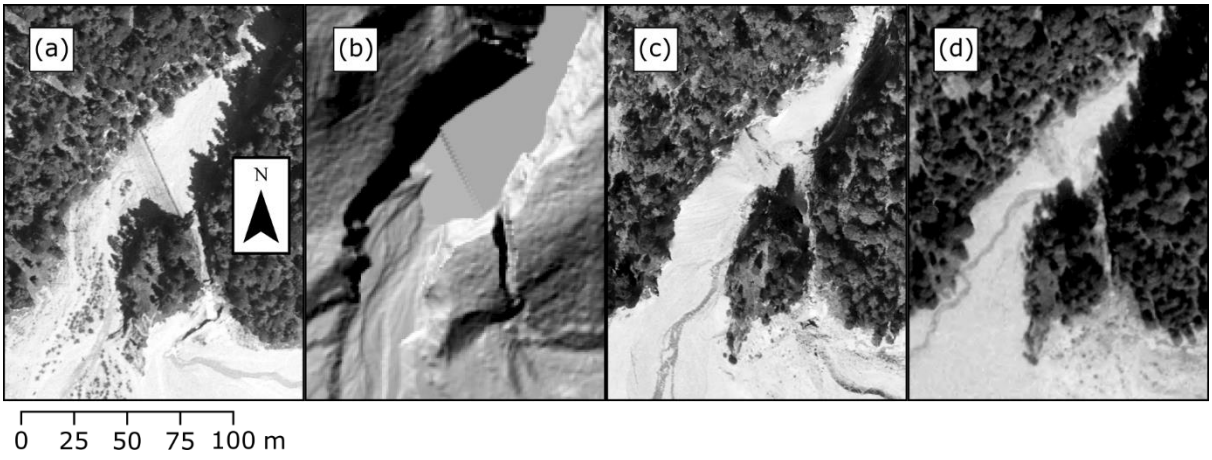

Figure 4: Franzosenmauer dam and sediment storage. (a): intact dam in 1960, (b): geometrical model of dam and sediment storage based on the 2019 DEM, (c): remainder of the dam in 1973 and (d): in 1977. Data source: Bayerische Vermessungsverwaltung

Following the dambreak event until the early 1980s, the main stream course was directed towards the south. The active floodplain migrated towards the west, leading to the activation of the southwestern fan toe for the first time since at least the late 1820s (LDBV, 1826, 1835, 1880, 1912, 1923) and the decoupling of the Nudelgraben in the 2010s. The westward shift of the active area continued until 2015, when the direction of the migration reversed from east-west to west-east. Between 2022 and 2024, a continuous north-south-oriented channel traversing the whole fan from apex to toe formed.

https://doi.org/10.5194/egusphere-2026-1699
Preprint. Discussion started: 13 April 2026

4.2.2 Climatic forcing of active area and regional comparison

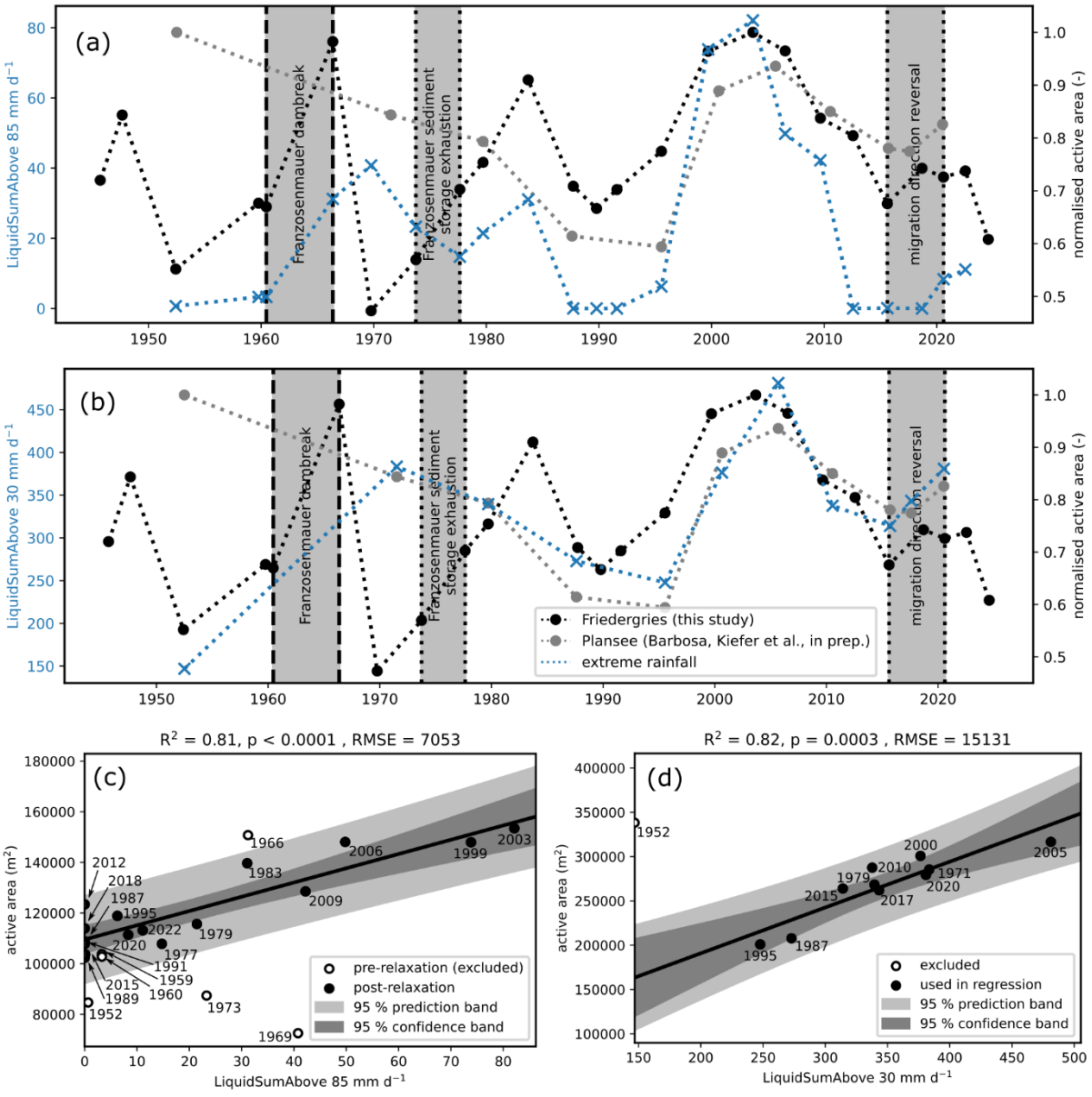

Figure 5: Comparison of the active areas at Friedergries and Plansee and regional heavy precipitation since 1945. (a): active area at Friedergries and Plansee with 5-years sum above 85 mm d^{-1} (best-fit model for Friedergries), (b): active area at Friedergries and Plansee with 5-years sum above 30 mm d^{-1} (best-fit model for Plansee), (c): linear regression of active area at Friedergries on 5-years sum above 85 mm d^{-1}, (d): linear regression of active area at Plansee on 5-years sum above 30 mm d^{-1}.

https://doi.org/10.5194/egusphere-2026-1699
Preprint. Discussion started: 13 April 2026

While the temporally sparse records prior to the 1980s differ widely, active area at Friedergries and Plansee show similar trends from the 1980s (Figure 5a, b). The regional heavy precipitation shows a similar trend to active area at Friedergries since the 1970s. Of the four precipitation statistics tested, only precipitation sum above a threshold and liquid precipitation sum above a threshold show satisfactory model performance. While precipitation sum above a threshold has the best overall explanatory power for active area at Friedergries (R^2 = 0.83), it performs worse for Plansee (R^2 = 0.65). In contrast, liquid precipitation sum above a threshold performs very well (R^2 > 0.80) for both catchments. Therefore, we focus our analysis and interpretation on liquid precipitation sum above a threshold. At Friedergries, the five-year liquid sum above 85 mm d^{-1} correlates best with active area (R^2 = 0.81, p < 0.0001; Figure 5c). At Plansee, the five-year liquid sum above 30 mm d^{-1} correlates best with active area (R^2 = 0.82, p = 0.0003; Figure 5d). Our sensitivity analysis indicates that these results are robust (Appendix E).

Daily precipitation of more than 30 mm occurs on 5-12 days each year depending on the station (EHR: 4.6 d yr^{-1}, GAP: 5.2 d yr^{-1}, REU: 5.7 d yr^{-1}, BER: 6.2 d yr^{-1}, ELI: 9.0 d yr^{-1}, ZUG: 12.3 d yr^{-1}). Daily precipitation exceeding 85 mm has a return interval of about 3–20 years depending on the station in question (ELI: 3.6 yrs, REU: 3.9 yrs, ZUG: 6.8 yrs, BER: 6.8 yrs, GAP: 15.5 yrs, EHR: 19.2 yrs; for full magnitude-frequency distributions, see Appendix C). It is noteworthy that these figures represent the return interval of the threshold. The return intervals of the rainfall events causing active area expansion are generally considerably higher, e.g. the 1-day return intervals of the 1977 and 2005 extreme events were approximately 20 yrs and 65 yrs at GAP, respectively.

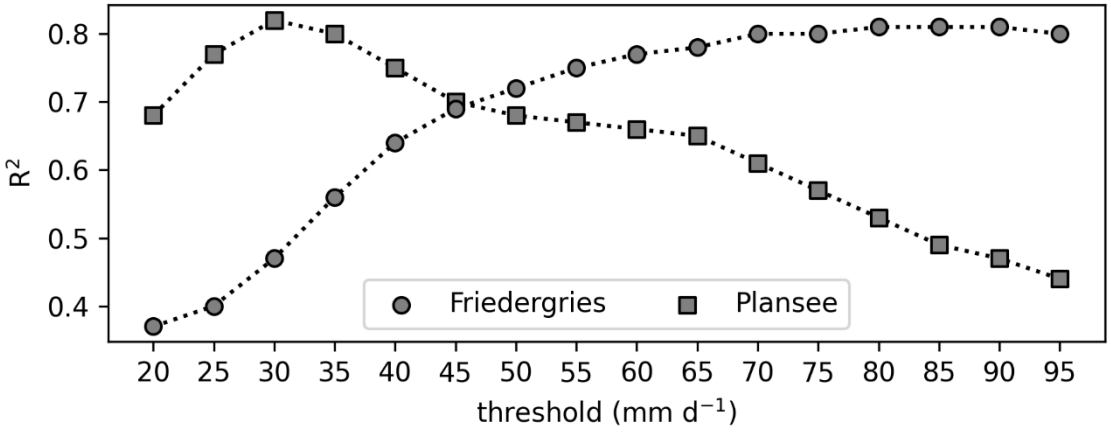

Figure 6: Model performance as a function of precipitation intensity threshold. For Plansee, the model performs best for a threshold of 30 mm d^{-1}, at Friedergries for an intensity threshold of 85 mm d^{-1}.

https://doi.org/10.5194/egusphere-2026-1699
Preprint. Discussion started: 13 April 2026

The peak in active area in the 1970s and 1980s at Friedergries is mostly attributable to three heavy precipitation events in 1977, 1979 and 1981. While the precipitation events in 1977 and 1981 affected the wider region (see Sect. 2), the 1979 event has not been described in the hydrographic literature of Austria (Hydrographischer Dienst Österreich, 1982). However, it led to heavy precipitation in northeastern Switzerland (Schweizerische Meteorologische Anstalt, 1979). These rain events account for 30–70% of the 5-year liquid precipitation above 85 mm d^{-1} at Friedergries (Table F1). In contrast, their contribution at Plansee is only 15–20% due to its lower threshold of 30 mm d^{-1} (Table F2). The peak of active area in the 2000s at Friedergries is attributable to the Whitsuntide flood 1999 and the August flood 2005 which together account for 94–100% of 5-year liquid precipitation above 85 mm d^{-1} at Friedergries, with the August 2002 flood accounting for the remainder (Table F1). Again, the importance of these rain events at Plansee is much lower with a contribution of 20–35% (Table F2).

4.3 Sub-annual to annual sediment redistribution

4.3.1 Volumetric change detections

Eight out of 16 epochs show net erosion exceeding uncertainty, five show net deposition (Figure 7, last row). Overall net change of –1000 ± 8300 m^3 remains indeterminate. On average, epochs of net deposition deposit twice as much sediment (4500 m^3 ± 2700 m^3; mean ± 1 standard deviation) as epochs of net erosion erode (–2100 m^3 ± 1900 m^3). Epochs of net erosion/deposition show no apparent link to season.

The change detection over the total time of investigation (last column in Figure 7) is consistent with the boundary between erosion and deposition zone determined by the inflection point. However, for each single epoch the boundary between the two zones can fluctuate considerably: in years with strong overall deposition, net accumulation can occur over the whole fan (e.g. epochs 5 and 10). Likewise, erosion can occur all the way to the fan toe (e.g. epoch 15). However, locally some accumulation occurred during all epochs, also in overall strongly erosive epochs (e.g. epochs 13 and 14).

https://doi.org/10.5194/egusphere-2026-1699
Preprint. Discussion started: 13 April 2026

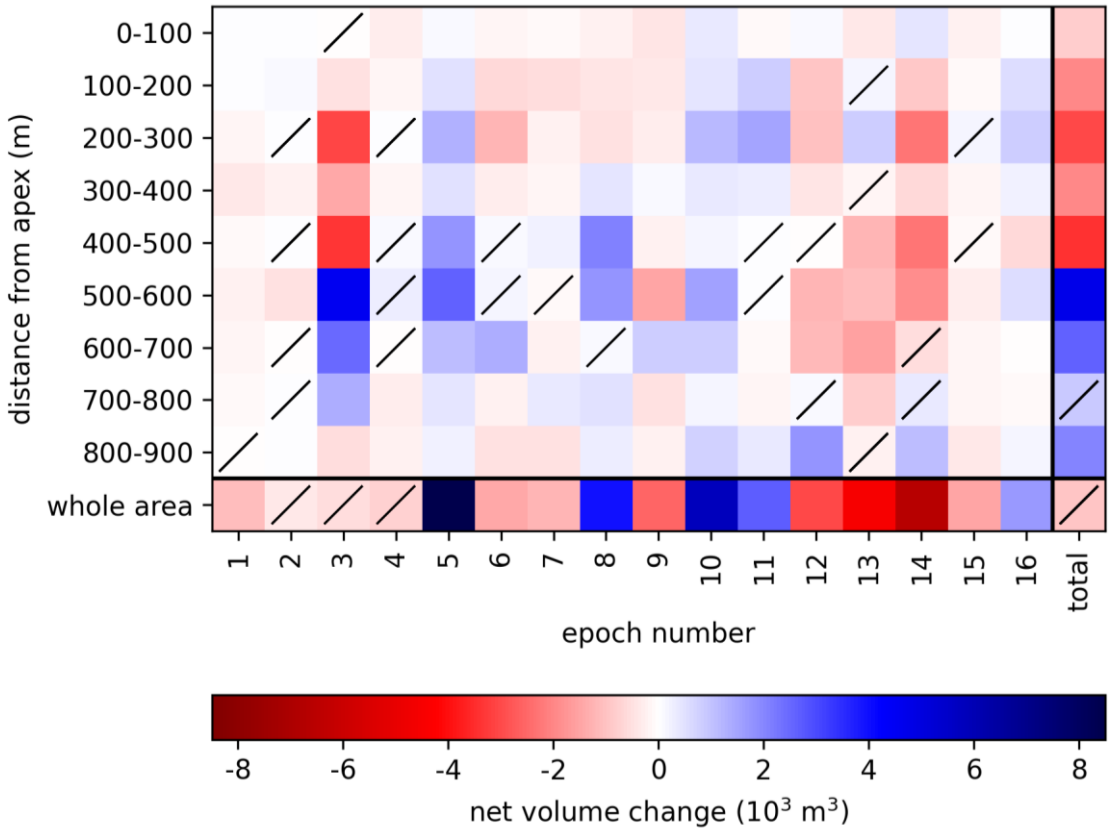

Figure 7: Net changes for UAV-based geomorphic change detections. Cells marked "/" have an uncertainty exceeding net change. The lowermost row shows net change for each epoch, the rightmost column shows net change over the whole epoch for each ring. The lower right corner of the diagram shows net change for the whole timespan.

375

4.3.2 Links between precipitation and volumetric sediment redistribution

Total liquid precipitation above 10 mm d^{-1} (Figure 8a, b) and total precipitation above 10 mm d^{-1} (Figure 8c, d) have a similar explanatory power for erosion and deposition.

https://doi.org/10.5194/egusphere-2026-1699
Preprint. Discussion started: 13 April 2026

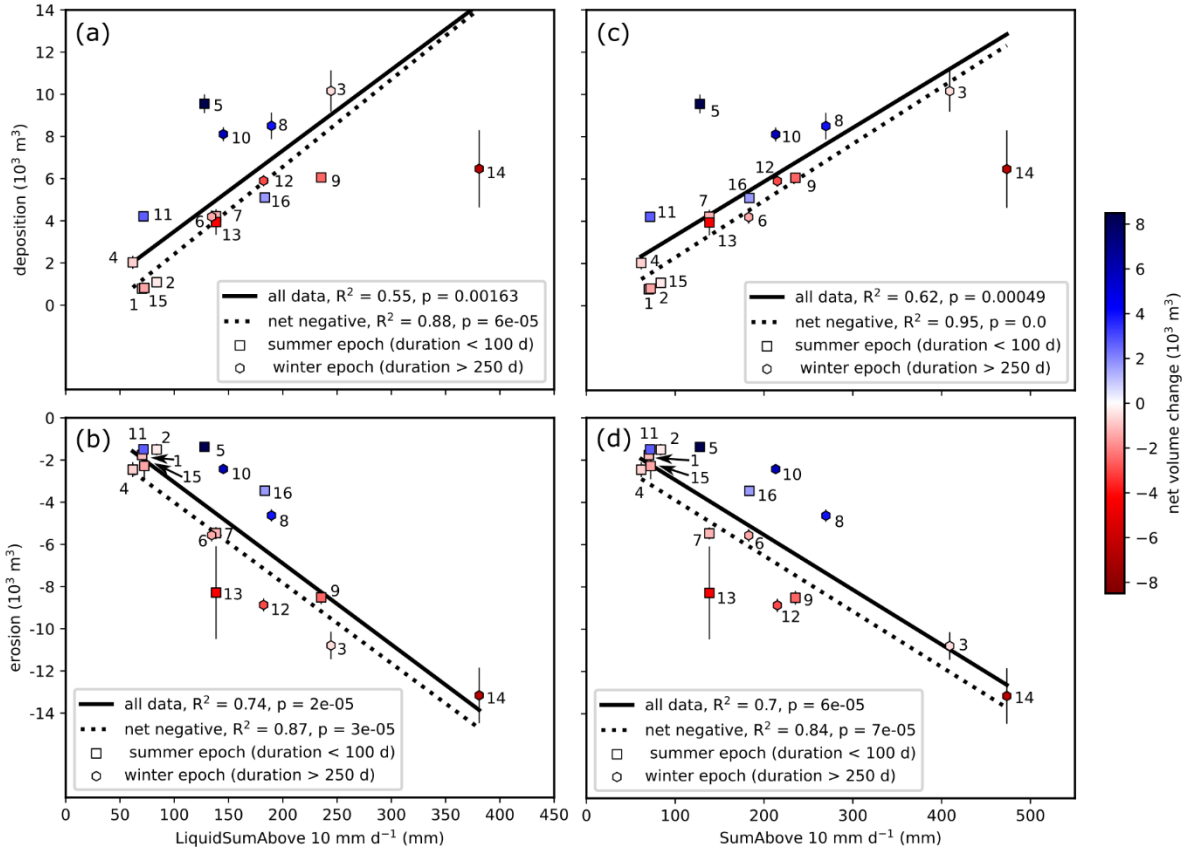

Figure 8: Relation between heavy precipitation and volumetric sediment redistribution. (a): Total rainfall above 10 mm d^{-1} vs. deposition. (b): Total rainfall above 10 mm d^{-1} vs. erosion, (c): Total precipitation (rain and snow) above 10 mm d^{-1} vs. deposition, (d): Total precipitation above 10 mm d^{-1} vs. erosion. In (a) and (c), epoch 14 was excluded from the linear regression because the area of deposition extended beyond the area captured during UAV flight campaigns.

Epochs of net erosion are well represented by the linear models while epochs of net deposition are conspicuous outliers. This is especially true for the relationship between precipitation and erosion (Figure 8b, d). The short summer epochs (squares in Figure 8) and the long winter epochs (hexagons) are equally well represented by the linear models. While the best fit lines are quite similar regardless of if all data or only the net negative epochs were used for regression, the coefficient of determination is higher in the "net negative" scenario both for erosion and deposition. The models predict higher erosion than deposition for any given amount of precipitation which is consistent with the observation that in most epochs, net volume change was negative (Figure 7).

https://doi.org/10.5194/egusphere-2026-1699
Preprint. Discussion started: 13 April 2026

4.3.3 Autogenic cycles of channel incision and backfill

In the UAV change detections, we observe five cycles of channel incision and backfill (Figure 9). Each of these cycles is associated with a small channel avulsion downstream of the fanhead trench. Considering the uncertainties associated with the timing of incision and backfill, each cycle is completed in less than one year. This does not apply for cycle 5, where backfill is far from complete. However, even in this case the onset of backfill occurs less than one year after incision. There is no link of incision/backfill to change detection epochs with net erosion/accumulation. In contrast, there is a clear seasonal signal with incision always occurring during the long winter change detection epochs and backfill during the short summer change detection epochs.

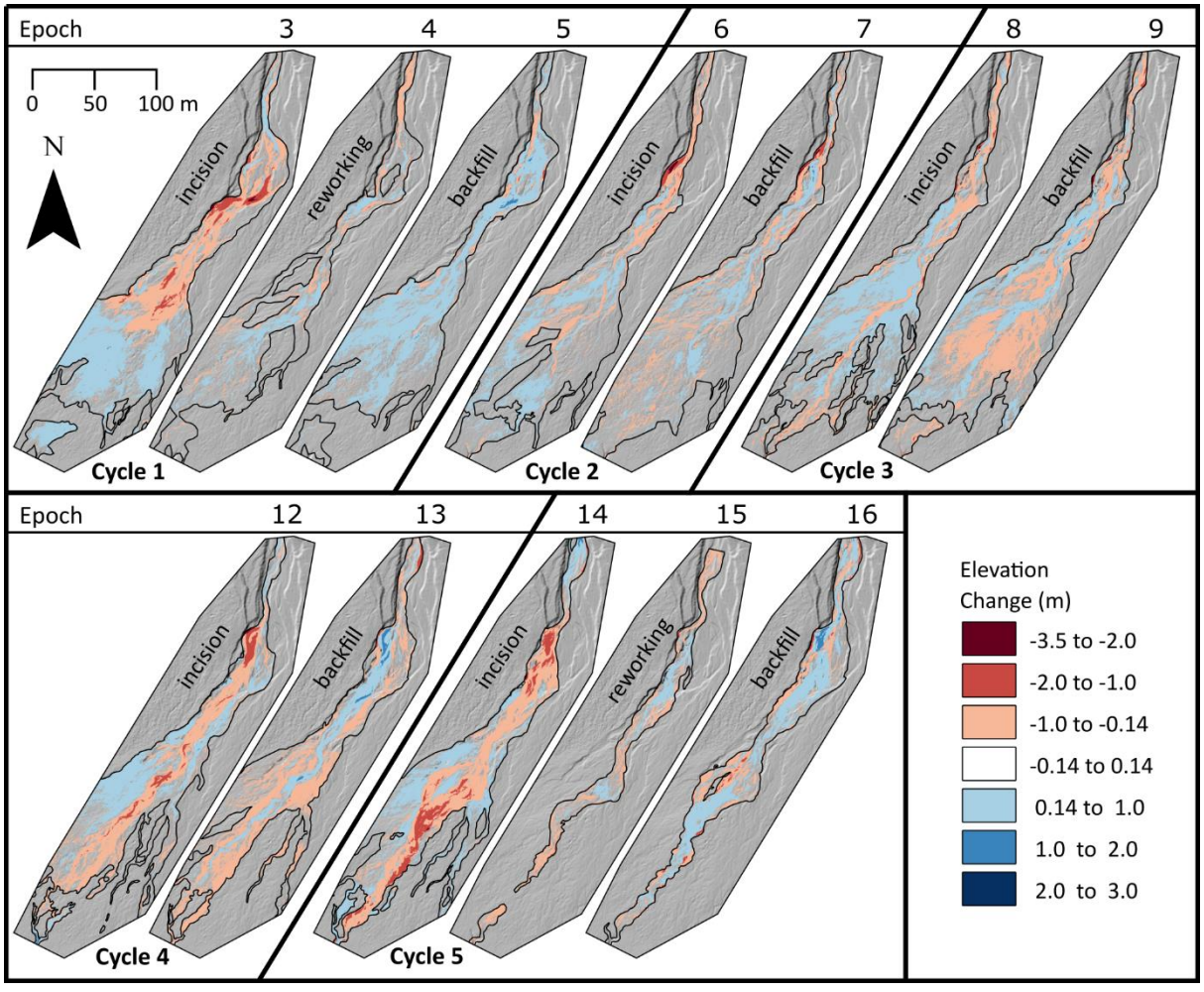

Figure 9: Cycles of incision and backfill. A memory effect is visible, where newly incised channels are infilled in subsequent epochs.

https://doi.org/10.5194/egusphere-2026-1699
Preprint. Discussion started: 13 April 2026

5 Discussion

5.1 Decadal sediment redistribution chronology

Based on the orthophoto interpretation and published reports, we derive a sediment redistribution chronology at Friedergries: from the construction of the dams in the 1930s and 1940s (Doposcheg, 1938; Kortenhaus, 1987) until the Franzosenmauer dambreak in the 1960s, sediment redistribution dynamics were determined by internal factors, i.e. the presence of the Franzosenmauer dam. This inference is strengthened by the observation that in our weather data analysis, we detect no apparent link to precipitation. After the dambreak event, the system took about 15 years to adjust to the new morphological state. This relaxation time is in the range of relaxation times reported for extreme events observed in comparable catchments (Rainato et al., 2025; Milan & Schwendel, 2021; East & Sankey, 2020; Morche & Schmidt, 2011; Bathurst & Ashiq, 1998). We infer that the long duration at Friedergries was caused by the gradual depletion of the 24000–36000 m^3 of sediment stored upstream of the dam, overprinting the rainfall–active area relationship (East et al., 2017). Thus, sediment dynamics continued to be determined by internal factors until sediment exhaustion of the reservoir was mostly complete in the mid-1970s. From the 1970s until 2023, heavy rainfall events determined sediment dynamics. During this time, active area dynamics at Friedergries and Plansee show a similar trend. As local controls like channel morphology and intra-catchment processes cannot explain the similar behavior, we attribute these similarities to regional weather patterns. Between 2023 and 2024, the incision of a continuous central channel induced another disturbance, where the system may either revert to the pre-incision dynamic equilibrium (if backfill of the central channel is completed) or develop a new post-incision dynamic equilibrium (signifying a system state change, cf. Milan & Schwendel, 2021; Phillips & van Dyke, 2016) characterized by efficient sediment routing along the central channel (Harvey, 2011).

5.2 Climatic forcing of sediment redistribution

5.2.1 Regional climatic forcing of active area

Weather data analysis confirms our inference that the subparallel evolution of active area at Friedergries and Plansee starting in the 1980s can be explained by regional weather. We identify liquid heavy precipitation as a suitable variable to describe this forcing. The observation that for the Plansee data, a precipitation threshold of 30 mm d^{-1} gives the best model performance while at Friedergries, a threshold of 85 mm d^{-1} gives the best model performance, indicates a higher susceptibility of the Plansee catchments towards heavy rainfall. As a consequence of the differing susceptibilities, Friedergries active area dynamics are mainly determined by supra-regional heavy precipitation events, while active area dynamics at Plansee are more sensitive towards local precipitation events.

https://doi.org/10.5194/egusphere-2026-1699
Preprint. Discussion started: 13 April 2026

5.2.2 Local climatic forcing of volumetric sediment redistribution

Sediment fan dynamics are a function of runoff, sediment input, and morphology including sediment characteristics (Lane & Richards, 1996; Milan, 2021). Using precipitation as a proxy for runoff, we interpret the linear models as representing the influence of the runoff component under conditions of low or constant background sediment input.

While total sediment input from the catchment remains unknown in our study, during epochs of net positive volume change, considerable sediment input must have taken place. We interpret these sediment input events as the arrival of sediment waves (cf. Barbosa et al., 2024) triggered in the catchment during extreme precipitation events. Due to their travel time of up to several years (Barbosa et al., 2024), the response of a fan system to a heavy precipitation event is twofold: while the fan responds immediately by incision, the sediments eroded in the catchment during the same event only arrive at the fan after a lag time which is determined by the catchment's and sediment's properties such as coupling of the sediment cascade (Milan & Schwendel, 2021; Rainato et al., 2018a), transport distance to the fan apex, and sediment grain-size distribution (Pellegrini et al., 2025; Oss Cazzador et al., 2021; Rainato et al., 2018b). Thus, it seems plausible that the reaction of the fan to heavy precipitation (sediment export during net negative epochs) is well predictable from precipitation, while the reaction of the catchment (sediment input during net positive epochs) overprints the precipitation–sediment redistribution relationship (East et al., 2017).

Based solely on the model performance (R^2), it is impossible to decide whether total precipitation above 10 mm d^{-1} or total liquid precipitation above 10 mm d^{-1} is the better explanatory variable. Both variables afford a physically meaningful explanation: An argument in favor of using only liquid precipitation is that only rain will directly be transformed into runoff. However, snow can be a substantial contributor to runoff and sediment transport during the melt season (Rainato et al., 2025; van Hamel et al., 2025; Lana-Renault et al., 2011). At Friedergries, snowmelt in the catchment is generally completed by mid-May. Our winter change detection epochs (hexagons in Figure 8) generally span the timeframe September-June and thus comprise the whole snow season. Therefore, it is reasonable to assume that all precipitation (rain and snow) is transformed into runoff and potentially contributes to sediment redistribution during winter change detection epochs.

The different thresholds of precipitation in the models of active area and volumetric sediment redistributions are easily explained by the different characteristics of active area and erosion/deposition volumes: active area only increases during extreme precipitation events that generate runoff exceeding the capacity of the active channel and floodplain. In contrast, DoD analyses also detect sediment redistribution in the channel or on the active floodplain, thus capturing the influence of lower magnitude precipitation events.

5.3 Modulation of external forcing by catchment morphology and autogenic cycles

The higher susceptibility of the Plansee catchments for heavy rainfall is likely explained by differing catchment characteristics: catchments at Plansee are smaller than the Friederlaine catchments and have higher channel gradients, which leads to relatively higher peak runoff (Liebscher, 1996). Additionally, the larger Friederlaine catchment can be expected to be characterized by

https://doi.org/10.5194/egusphere-2026-1699
Preprint. Discussion started: 13 April 2026

more efficient stream hydrological retention and in-catchment storage of sediment, in turn leading to lower discharge and sediment export compared to the Plansee catchments (Liebscher, 1996; Crosta & Frattini, 2004; Casper & Bormann, 2016). In contrast, the higher circularity of the Friederlaine catchment would tend to increase peak runoff more at Friedergries than at Plansee (Liebscher, 1996). However, circularity at Friedergries is well within the range of circularity at Plansee, barely exceeding the 75th percentile of the Plansee catchments. Therefore, we argue that the influence of circularity is negligible compared to catchment size, channel slope, and flow length.

We interpret the cycles of incision and backfill detected in the UAV change detections as small-scale autogenic cycles (cf. de Haas et al., 2016) similar to the memory effect observed for debris flows by de Haas et al. (2020) and for braided rivers by Bakker et al. (2019). Two alternative explanations for cycles of incision and backfill come to mind: sediment input from the catchment and seasonal dynamics of sediment transport (Rainato et al., 2025; Ariagno et al., 2022). However, incision and backfill are out of phase with epochs of net erosion and accumulation, respectively. Therefore, we argue that sediment input from the catchment is unlikely to be responsible for the observed cycles of channel incision and backfill. While the cycles of incision and backfill show a strong link to season, net changes show no apparent link to season. Therefore, we argue that seasonal differences in sediment availability are also unlikely to be the driver for cycles of incision and backfill. The most likely explanation is that these cycles are driven by internal feedbacks that redistribute sediment within the fan system and maintain its capability for rapid channel migration (Bakker et al., 2019).

The development of the continuous central channel between 2023 and 2024 which we interpret as the start of a fifth autogenic cycle represents a major change of the fan system. It remains to be seen whether the fan reverts to its previous dynamic equilibrium completing the fifth autogenic cycle or if the incision of the central channel constitutes a system state change (cf. Milan & Schwendel, 2021; Phillips & van Dyke, 2016).

5.4 Limitations of the study

An important limitation of our study is the lack of local precipitation and runoff data. For the analysis of sub-annual to annual sediment dynamics, this problem is less severe as high-resolution precipitation data from the weather station at Griesen c. 3.4 km south of the catchment is available. The linear models of erosion/deposition on precipitation above 10 mm d^{-1} show considerable sediment redistribution even for low precipitation amounts. However, taking into account the precipitation lapse rate of +6.8 mm km^{-1} for the Northern Calcareous Alps (Baumgartner et al., 1983), annual precipitation in the Friederlaine catchment can be expected to be about 500 mm higher than annual precipitation measured at Griesen. For decadal dynamics, on the other hand, local data neither exists for Plansee nor for Friedergries. We argue that this does not represent a severe issue for our research, as we specifically investigate the similar trends in active area at Friedergries and Plansee. As we interpret these trends as representing regional dynamics, it seems reasonable or even beneficial to investigate their link to regional weather patterns, taking into account data from several weather stations.

A severe limitation to our volumetric change detections is that we lack information on sediment input from the Friederlaine catchment. Therefore, all numbers presented in this study are minimum values of e.g. sediment export from the fan (in epochs

https://doi.org/10.5194/egusphere-2026-1699
Preprint. Discussion started: 13 April 2026

of net negative change) or sediment input from the catchment (in epochs of net positive change). Furthermore, we neglect antecedent conditions and catchment memory in our analysis. Viewed in a disposition-trigger framework (Kaitna et al., 2013), this means that we only investigate meteorological triggers of sediment redistribution. This is problematic as e.g. soil saturation due to antecedent rainfall or snowmelt plays a crucial role in discharge generation and sediment transport (Landesamt für Wasserwirtschaft, 2003; LfU, 2007). Additionally, snow cover impacts sediment availability (Schmidt et al., 2022) and is a prerequisite for rain-on-snow events, which can have severe geomorphic impacts (Beniston & Stoffel, 2016). Neglecting antecedent conditions may lead to an over-estimation of precipitation thresholds for sediment redistribution. This is likely less impactful at Friedergries, as antecedent conditions are less important for discharge generation due to extreme compared to moderate extreme precipitation (Brunner et al., 2021). Quantifying antecedent conditions would have required us to make a number of additional subjective choices in data analysis, e.g. the definition of the timeframe for which we calculate antecedent conditions. We prefer a potentially biased estimate of precipitation thresholds over results from an overly subjective data analysis strategy.

5.5 Fan evolution in a warming climate

The ongoing debate about alpine sediment fan dynamics in a warming climate is based on the inference that an increase in heavy precipitation may lead to elevated geomorphic activity (e.g. Turkington et al., 2016; Kiefer, Oswald et al., 2021; Kido et al., 2023; East & Sankey, 2023; East et al., 2017). However, several studies have shown that sediment redistribution will only increase long-term under transport-limited conditions, as the depletion of sediment storages may lead to a decrease in sediment yield from catchments (Hirschberger et al., 2021; Jomelli et al., 2007). Other authors have stressed the importance of connectivity for sediment transport through fluvial systems (Milan & Schwendel, 2021; Harvey, 2011). We argue that even if sediment storages in the catchment of a given sediment fan are exhausted or the fan is decoupled from its catchment in terms of bedload transport, sediment redistribution from the apex to the toe will increase in response to increasing heavy precipitation as the fan itself is a sediment storage that can be remobilized. However, catchment sediment storage depletion will result in rapid incision of the fan, as sediment export from the fan is no longer offset by sediment import from the catchment. This would result in a stabilization of the fan surface outside of the main channel and a loss of the sediment buffer capacity of the sediment fan (“throughfan trenching”, Harvey, 2011). For the Main Dolomite region of the Northern Calcareous Alps, we deem this possibility improbable due to large storages of loose debris and the high weathering rates (Sass et al., 2005; Bayerisches Geologisches Landesamt, 1996).

The projected increase of heavy precipitation events across all seasons until the end of the century (Giorgi et al., 2016; Gobiet et al., 2014; Estermann et al., 2025; Kotlarski et al., 2023) impacts both sediment redistribution and the potential for system state changes.

System state changes such as the 1960s dambreak event, potentially the incision of the continuous central channel between 2023 and 2024, and similar system state changes reported in the literature (Morche et al., 2006; Milan, 2012, 2021; Harvey, 1986, 2007) are more likely to occur in a climate with more frequent and severe precipitation events. This means that sediment

https://doi.org/10.5194/egusphere-2026-1699
Preprint. Discussion started: 13 April 2026

fan systems become less stable and predictable. Despite summer drying identified in most climate projections until the end of the century (e.g. Gobiet et al., 2014; Estermann et al., 2025; LfU, 2020; Kotlarski et al., 2023), large disturbances are still most likely to occur during the summer months when high temperatures render the atmosphere especially prone to extreme precipitation (Brönnimann et al., 2018). This is especially true for the mid-21st century when summer precipitation may increase due to an increase of convective rainstorms (Giorgi et al. 2016). However, system state changes will continue to be dependent on internal system characteristics like the coupling of the sediment cascade, which is illustrated by a regional example: While the August 2005 flood led to a system state change in the upper Partnach catchment owing to a dambreak event (Morche et al., 2007), the Friedergries merely reacted with an expansion of its active floodplain which was in line with its dynamics since the 1970s. This is likely to be explained by the observation that at Friedergries, the potential for a system state change was lower than in the upper Partnach catchment, where a dam decoupling the sediment cascade was present (Morche et al., 2007).

Extreme sediment redistribution events leading to a shift and/or expansion of active area on sediment fans are likely to increase as long as at least the lower part of the fan remains un-trenched. We infer that future active area dynamics will be modulated by catchment morphology: for small, steep catchments with short flow lengths and juvenile fans and cones, our results imply a shift of activity towards spring and autumn as moderate extreme precipitation with return intervals of up to one year will be more likely to occur in spring and autumn (Brönnimann et al., 2018). Such a shift towards spring and autumn is in line with inferences on debris flow activity (Stoffel et al., 2014; Kaitna et al., 2023). In contrast, larger, more gently inclined catchments with long flow lengths and mature fans will tend to retain their activity peak in summer, as changes of active area are driven by precipitation events exceeding several years that will be most likely to occur in summer also in the future (Brönnimann et al., 2018). This might be exacerbated by different scaling of moderate and extreme heavy precipitation events in response to a warming climate (Estermann et al., 2025; Brönnimann et al., 2018; Brunner et al., 2021). However, changes of seasonality are likely to be more complex than shown in our data as snow plays a crucial role for sediment availability (Schmidt et al., 2022), runoff (van Hamel et al., 2025; Beniston & Stoffel, 2016), and soil saturation (Landesamt für Wasserwirtschaft, 2003; LfU, 2007). For volumentric sediment redistribution, we postulate that both total redistribution and geomorphic work per sediment transport event will increase: while rainfall intensifies across all seasons (Giorgi et al., 2016; Gobiet et al., 2014; Estermann et al., 2025), annual rainfall is projected to stay about equal in the Bavarian Alps (LfU, 2020; Kotlarski et al., 2023). Thus, rainfall will be concentrated in less, but higher intensity events. This increases the probability of transport threshold exceedance, causing overall higher sediment redistribution. Additionally, higher intensity rainfall events will cause higher intensity sediment redistribution events, giving rise to less predictable sediment redistribution dynamics with a higher damage potential per event.

https://doi.org/10.5194/egusphere-2026-1699
Preprint. Discussion started: 13 April 2026

6 Conclusion and outlook

Our study disentangles the relative importance of external forcings and internal factors and thresholds for sediment fan dynamics. Specifically, we (i) derive a sediment redistribution chronology, (ii) quantify climatic forcing of sediment redistribution, (iii) detect and quantify autogenic behavior and system thresholds for the "model" alluvial fan Friedergries and (iv) decipher how catchment morphology and fan maturity shape future sediment fan dynamics in a changing climate.

For the Friedergries alluvial fan we show that periods of high and low floodplain activity alternated since 1945. Prior to the mid-1970s, a dam at the fan apex strongly influenced floodplain dynamics.

At both field sites, active area dynamics are closely linked to heavy rainfall. Active area dynamics at Friedergries are mainly determined by supra-regional precipitation events with return intervals exceeding several years, while at Plansee, smaller local events with return intervals below one year play a larger role.

Climatic forcing of sediment redistribution is overprinted by autogenic behavior and internal system characteristics both on the decadal and sub-annual timescale. Differing susceptibilities of Friedergries and Plansee to heavy precipitation are explained by catchment morphometry. For Friedergries, we detect five small-scale autogenic cycles governing time and place of channel incision and backfill.

Based on our findings and the literature, we make the following inferences about sediment fan evolution in a changing climate:

(1) Total sediment redistribution will increase in response to rainfall intensification.
(2) Geomorphic work per rainstorm will increase in response to rainfall concentration.
(3) System state changes will become more likely, rendering fan systems less stable and predictable.
(4) Sediment redistribution will shift towards spring and autumn in response to summer drying and a shift of moderate extreme rainfall towards spring and autumn (Brönnimann et al., 2018).
(5) Small, steep catchments with juvenile fans and cones will experience a more pronounced shift of activity towards spring and autumn than larger, gentler catchments with mature fans.

Data Availability. Official digital elevation models are available from the sources cited in Sect. 3.1. Weather data are publicly available from the sources cited in Table 1. Historical aerial imagery as well as historical topographic maps are available upon request from the Bavarian Landesamt für Digitalisierung, Breitband und Vermessung (LDBV), the Land Tirol Abteilung Geoinformation, and the Austrian Bundesamt für Eich- und Vermessungswesen (BEV). Digital surface models derived from uncrewed aerial imagery are part of an ongoing long-term monitoring project and will not be made publicly available before the end of this project. Active area data from Plansee will shortly be published in Barbosa, Kiefer et al. (currently in preparation).

https://doi.org/10.5194/egusphere-2026-1699
Preprint. Discussion started: 13 April 2026

Appendix A: UAV change detection epochs

Table A1: Characteristics of the UAV change detection epochs.

epoch	start	end	duration (d)	season
1	11.06.2018	18.07.2018	37	summer
2	18.07.2018	11.09.2018	55	summer
3	11.09.2018	27.06.2019	289	winter
4	27.06.2019	05.08.2019	39	summer
5	05.08.2019	10.09.2019	36	summer
6	10.09.2019	19.05.2020	252	winter
7	19.05.2020	14.07.2020	56	summer
8	14.07.2020	01.06.2021	322	winter
9	01.06.2021	07.09.2021	98	summer
10	07.09.2021	30.06.2022	296	winter
11	30.06.2022	30.08.2022	61	summer
12	30.08.2022	28.06.2023	302	winter
13	28.06.2023	08.08.2023	41	summer
14	08.08.2023	29.06.2024	326	winter
15	29.06.2024	09.08.2024	41	summer
16	09.08.2024	29.10.2024	81	summer

Appendix B: Historical aerial imagery camera precalibration

We use the frame camera model (Agisoft, 2025), assuming that radial distortion can be modelled by three distortion parameters (the standard assumption in Metashape; Over et al., 2021) and that tangential distortion is negligible. Under these assumptions it can be shown that:

$$\Delta r = K_1 r^3 + K_2 r^5 + K_3 r^7$$

With Δr: radial distance between a point in a distortion-free image and the same point in an image with radial distortion (measured in pixels), K_1, K_2, K_3: radial distortion parameters (dimensionless). We use ordinary least squares inversion to estimate the distortion parameters based on calibration reports for the aerial imagery.

https://doi.org/10.5194/egusphere-2026-1699
Preprint. Discussion started: 13 April 2026

Appendix C: 1-day return intervals

We model return intervals with an exponential distribution of the form (DWA, 2012):

$$h_N(T_n) = u + w \cdot \ln(T_n)$$

With h_N: 1-day precipitation sum (mm), T_n: return interval (a), u, w: model parameters of the exponential distribution function.

Table C1: Model parameters, R^2, and p-value of the fits for the respective weather stations.

Station	u	w	R^2	p
BER	49.7368	18.3949	0.90	< 0.0001
EHR	45.4895	13.3801	0.90	< 0.0001
ELI	60.8503	18.8590	0.98	< 0.0001
GAP	47.2342	13.7789	0.93	< 0.0001
REU	53.5295	23.2676	0.87	< 0.0001
ZUG	60.5343	12.7555	0.94	< 0.0001

Appendix D: Uncertainty propagation for change detections

The matrix notation of uncertainty propagation is given by (Vermeesch, 2017):

$$\sigma_f^2 = J\,V\,J^T$$

With σ_f^2: propagated uncertainty, J: Jacobian matrix, V: variance-covariance matrix. In the case of summation, $J = [1 \quad 1 \quad \cdots \quad 1]$.

It can be shown that the variance-covariance matrix can be written as (Dodge, 2008; Ku, 1966):

$$V = \begin{bmatrix} STD(x_1)^2 & r_{12}STD(x_1)STD(x_2) & \cdots & r_{1n}STD(x_1)STD(x_n) \\ r_{21}STD(x_2)STD(x_1) & STD(x_2)^2 & \cdots & r_{12}STD(x_2)STD(x_n) \\ \vdots & \vdots & \ddots & \vdots \\ r_{n1}STD(x_n)STD(x_1) & r_{n2}STD(x_n)STD(x_2) & \cdots & STD(x_n)^2 \end{bmatrix}$$

With $STD(x_i)$: uncertainty of net change of DoD_i, r_{ij}: Pearson's r between DoD_i and DoD_j (Ku, 1966).

This can be written as:

$$V = M \circ R$$

With

https://doi.org/10.5194/egusphere-2026-1699
Preprint. Discussion started: 13 April 2026

$$M = \begin{bmatrix} STD(x_1)^2 & STD(x_1)STD(x_2) & \cdots & STD(x_1)STD(x_n) \\ STD(x_2)STD(x_1) & STD(x_2)^2 & \cdots & STD(x_2)STD(x_n) \\ \vdots & \vdots & \ddots & \vdots \\ STD(x_n)STD(x_1) & STD(x_n)STD(x_2) & \cdots & STD(x_n)^2 \end{bmatrix}$$

And

$$R = \begin{bmatrix} 1 & r_{12} & \cdots & r_{1n} \\ r_{21} & 1 & \cdots & r_{2n} \\ \vdots & \vdots & \ddots & \vdots \\ r_{n1} & r_{n2} & \cdots & 1 \end{bmatrix}$$

Two consecutive DoDs "share" one out of two DEMs (e.g. the DEM from August 2019 is used both in the calculation of the DoD from June to August 2019 and for the DoD from August 2019 to September 2019), so we assume that their uncertainties are correlated with an $r = 0.5$. In contrast, we assume that uncertainties of non-consecutive DoDs (which "share" no DEM) are uncorrelated. Consequently:

$$R = \begin{bmatrix} 1 & 0.5 & 0 & 0 & \cdots & 0 \\ 0.5 & 1 & 0.5 & 0 & \cdots & 0 \\ 0 & 0.5 & 1 & 0.5 & \cdots & 0 \\ 0 & 0 & 0.5 & 1 & \cdots & 0.5 \\ \vdots & \vdots & \vdots & \vdots & \ddots & \vdots \\ 0 & 0 & 0 & 0.5 & \cdots & 1 \end{bmatrix}$$

https://doi.org/10.5194/egusphere-2026-1699
Preprint. Discussion started: 13 April 2026

Appendix E: Sensitivity analysis for the choice of weathering timespan

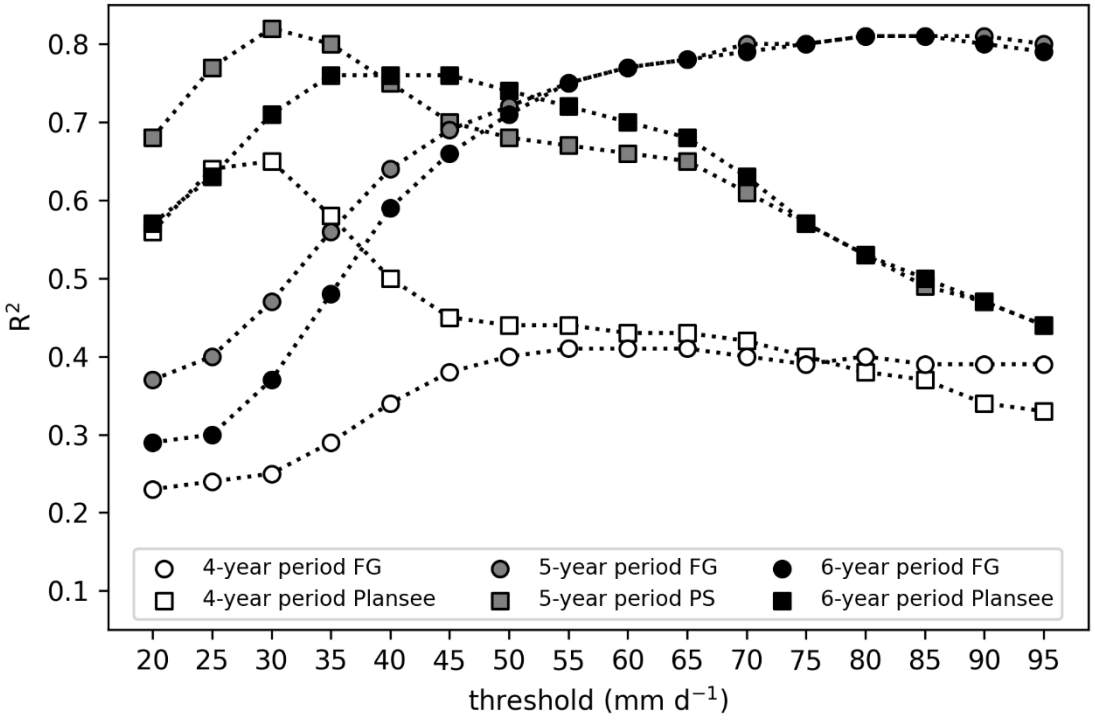

Figure E1: Sensitivity of model performance for the choice of weathering timespan and precipitation threshold for OLS linear regressions based on liquid precipitation sum above a threshold. For the 4-year period, model performance is not satisfying. 6- and 7-year periods consistently predict higher thresholds at Friedergries than at Plansee.

Table E1: Precipitation threshold associated with peak model performance.

	Friedergries		Plansee	
	Threshold (mm d^{-1})	R^2 (%)	Threshold (mm d^{-1})	R^2 (%)
4-year period	60	41.46	30	65.20
5-year period	85	81.50	30	81.57
6-year period	80	81.30	40	76.17

https://doi.org/10.5194/egusphere-2026-1699
Preprint. Discussion started: 13 April 2026

Using a 4-year weathering timespan does not yield satisfactory model performances (Figure E1, Table E1). Models employing 5- and 6-year weathering timespans perform similar in terms of R^2. While they yield slightly different thresholds for peak model performance, the overall trend of a high threshold at Friedergries compared to a low threshold at Plansee remains.

Appendix F: Contribution of notable heavy rainfall events to planimetric activity peaks

Table F1: Contribution of notable heavy rainfall events to 5-year liquid precipitation above 85 mm d^{-1} at Friedergries. Note that because of the 5-year weathering timespan required to visibly darken inactive sediments in aerial imagery, the impact of a given heavy precipitation event is detectable on aerial imagery captured up to 5 years later.

Year of flight	July rainstorm 1977 (31.07.1977)	June rainstorm 1979 (16.-17.06.1979)	July rainstorm 1981 (18.-19.07.1981)	Whitsuntide flood 1999 (20.-22.05.1999)	August 2002 flood (11.08.2002)	August flood 2005 (22.08.2005)
1977	60 %					
1979	34 %	43 %				
1983		29 %	71 %			
1999				100 %		
2003				97 %	3 %	
2006					6 %	94 %
2009						100 %

Table F2: Contribution of notable heavy rainfall events to 5-year liquid precipitation above 30 mm d^{-1} at Plansee. Note that because of the 5-year weathering timespan required to visibly darken inactive sediments in aerial imagery, the impact of a given heavy precipitation event is detectable on aerial imagery captured up to 5 years later.

Year of flight	July rainstorm 1977 (31.07.1977)	June rainstorm 1979 (16.-17.06.1979)	July rainstorm 1981 (18.-19.07.1981)	Whitsuntide flood 1999 (20.-22.05.1999)	August 2002 flood (11.08.2002)	August flood 2005 (22.08.2005)
1979	14 %	22 %				
2000				35 %		
2005					9 %	19 %
2010						26 %

https://doi.org/10.5194/egusphere-2026-1699
Preprint. Discussion started: 13 April 2026

Author contributions. MK conceptualized and supervised the research. PG and MK acquired the funding, MK and TW provided resources. PG and TW developed the methodology. TW acquired and processed the UAV data, PG performed all other analyses. PG wrote the initial draft, PG, TW and MK reviewed and edited the final draft.

Competing interests. MK is an associate editor of Earth Surface Dynamics.

Acknowledgements. We want to especially thank Natalie Barbosa and Carolin Kiefer for sharing and discussing their Plansee data. The authors are indebted to Forstbetrieb Oberammergau for granting access to their private roads and to the Regierung von Oberbayern for permitting UAV flights in the Natural Reserve Friedergries. We thank LDBV, BEV and Land Tirol Abteilung Geoinformation for supplying the historical aerial imagery at heavily discounted cost. PG thanks Natalie Barbosa and Lukas Lucks for sharing their knowledge on photogrammetric processing and the employees of the LDBV and Land Tirol Abteilung Geoinformation for answering detailed questions on historical aerial imagery metadata. PG thanks Benjamin Jacobs for fruitful discussions on geomorphic change detections.

Financial support. During the work on this study, PG received a scholarship from the Studienstiftung des Deutschen Volkes.

References

Achilleos, G.: The Inverse Distance Weighted interpolation method and error propagation mechanism – creating a DEM from an analogue topographical map, Journal of Spatial Science, (56), 283–304, https://doi.org/10.1080/14498596.2011.623348, 2011.

Agisoft: Metashape 2.2 Manual, 2025. Available at: https://www.agisoft.com/downloads/user-manuals/ (last access: 12 November 2025)

Anderson, S.W.: Uncertainty in quantitative analyses of topographic change: error propagation and the role of thresholding, Earth Surface Processes and Landforms, 44, 1015–1033. https://doi.org/10.1002/esp.4551, 2019.

Ariagno, C., Le Bouteiller, C., van der Beek, P. & Klotz, S.: Sediment export in marly badland catchments modulated by frost-cracking intensity, Draix-Bléone Critical Zone Observatory, SE France, Earth Surface Dynamics, 10, 81–96, https://doi.org/10.5194/esurf-10-81-2022, 2022.

Aschwanden, H.: Hochwasser 1999. Analyse der Messdaten und statistische Einordnung, Schweizer Bundesamt für Wasser und Geologie, 2000. Available at: https://www.bafu.admin.ch/bafu/de/home/themen/wasser/publikationen-studien/publikationen-wasser/hochwasser-1999.html (Last accessed: 16.10.2025)

Bakker, M., Antoniazza, G., Odermatt, E. & Lane, S.: Morphological response of an alpine braided reach to sediment-laden flow events, Journal of Geophysical Research: Earth Surface, 124, 1310–1328, https://doi.org/10.1029/2018JF004811, 2019.

https://doi.org/10.5194/egusphere-2026-1699
Preprint. Discussion started: 13 April 2026

Barbosa, N.*, Kiefer, C.*, Jubanski, J., Siegert, F., & Krautblatter, M. (in preparation): Combined terrestrial and limnic record since 1950s deciphers massive debris flow activity and connectivity shift in a changing climate.

Barbosa, N., Leinauer, J., Jubanski, J., Dietze, M., Münzer, U., Siegert, F. & Krautblatter, M.: Massive sediment pulses triggered by a multi-stage 130 000 m^3 alpine cliff fall (Hochvogel, DE-AT), Earth Surface Dynamics, 12, 249–269, https://doi.org/10.5194/esurf-12-249-2024, 2024.

Bathurst, J.C. & Ashiq, M.: Dambreak flood impact on mountain stream bedload transport after 13 years, Earth Surface Processes and Landforms, 23, 643–649, https://doi.org/10.1002/(SICI)1096-9837(199807)23:7<643::AID-ESP889>3.0.CO;2-3, 1998.

Baumgartner, A., Reichel, E. & Weber, G.: Der Wasserhaushalt der Alpen: Niederschlag, Verdunstung, Abfluß und Gletscherspende der Alpen im Jahresdurchschnitt für die Normalperiode 1931-1960, Oldenbourg Wissenschaftsverlag, München/ Wien,343 pp., ISBN 3486272519, 1983.

Bayerisches Geologisches Landesamt: Erläuterungen zur geologischen Karte von Bayern 1:500000, Bayerisches Geologisches Landesamt, München, 329 pp., 1998.

Beniston, M. & Stoffel, M. (2016): Rain-on-snow events, floods and climate change in the Alps: Events may increase with warming up to 4°C and decrease thereafter, Science of the Total Environment, 571, 228–236. https://doi.org/10.1016/j.scitotenv.2016.07.146, 2016.

Bezzola, G.R. & Hegg, C.: Ereignisanalyse Hochwasser 2005. Teil 1: Prozesse, Schäden und erste Einordnung, Schweizer Bundesamt für Umwelt, Bern, 215 pp., 2007.

BMLUK: WebGIS Applikation eHYD, https://ehyd.gv.at/ (last access 16 October 2025)

Brönnimann, S., Rajczak, J., Fischer, E.M., Raible, C.C., Rohrer, M. & Schär, C.: Changing seasonality of moderate and extreme precipitation events in the Alps, Natural Hazards and Earth System Sciences, 18, 2047–2056, https://doi.org/10.5194/nhess-18-2047-2018., 2018.

Brunner, M.I., Swain, D.L., Wood, R.R., Willkofer, F., Done, J.M., Gilleland, E. & Ludwig, R.: An extremeness threshold determines the regional response of floods to changes in rainfall extremes, Communications Earth & Environment, 2, 173, https://doi.org/10.1038/s43247-021-00248-x, 2021.

Burrough, P.A. and McDonnell, R.A.: Principles of Geographical Information Systems, Oxford University Press, Oxford, 333 pp., ISBN 0198233663, 1998.

Caine, N.: The rainfall intensity-duration control of shallow landslides and debris flows, Geogr. Ann. 62 A (1-2), 23–27, https://doi.org/10.2307/520449, 1980.

Casper & Bormann (2016): Abfluss im Gewässersystem, in: Hydrologie, 1st edition, edited by: Fohrer, N., Bormann, H., Miegel, K., Casper, M., Bronstert, A., Schumann, A. and Weiler, M., Haupt, Bern, 127–142, ISBN 9783825245139, 2016.

https://doi.org/10.5194/egusphere-2026-1699
Preprint. Discussion started: 13 April 2026

Chiverrell, R. & Jakob, M. (2013): Radiocarbon dating: alluvial/debris cone evolution and hazards, in: Dating torrential processes on fans and cones, edited by: Schneuwly-Bollschweiler, M., Stoffel, M. & Rudolf-Miklau, F., Springer, Dordrecht, 265–282, https://doi.org/10.1007/978-94-007-4336-6_17, 2013.

Crosta, G.B. & Frattini, P. (2004): Controls on modern alluvial fan processes in the Central Alps, Northern Italy, Earth Surface Processes and Landforms, 29, 267–293, https://doi.org/10.1002/esp.1009, 2004.

De Haas, T., Nijland, W., de Jong, S.M., McArdell, B.W.: How memory effects, check dams, and channel geometry control erosion and deposition by debris flows, Scientific Reports, 10, 14024, https://doi.org/10.1038/s41598-020-71016-8, 2020.

De Haas, T., van den Berg, W., Braat, L. & Kleinhans, M. G.: Autogenic avulsion, channelization and backfilling dynamics of debris-flow fans, Sedimentology, 63: 1596–1619, https://doi.org/10.1111/sed.12275, 2016

Dodge, Y.: Variance-Covariance Matrix, in: The Concise Encyclopedia of Statistics, Springer, New York, 559–561, https://doi.org/10.1007/978-0-387-32833-1, 2008.

Doposcheg, J. (1938): Berge und Pflanzen (Werden und Wachsen) in der Landschaft Werdenfels, Verlag A. Adam, Garmisch, 453 pp., 1938.

DWA: Arbeitsblatt DWA-A 531. Starkregen in Abhängigkeit von Wiederkehrzeit und Dauer, Deutsche Vereinigung für Wasserwirtschaft, Abwasser und Abfall e.V., Hennef, 29 pp., 2012.

DWD: Opendata DWD, https://opendata.dwd.de/, last access 16 October 2025.

East, A.E., Jenkins, K.J, Happe, P.J., Bountry, J.A., Beechie, T.J., Mastin, M.C., Sankey, J.B. & Randle, T.J.: Channel-planform evolution in four rivers of Olympic National Park, Washington, USA: the roles of physical drivers and trophic cascades, Earth System Processes and Landforms, 42, 1011–1032. https://doi.org/10.1002/esp.4048, 2017.

East, A.E. & Sankey, J.B.: Geomorphic and sedimentary effects of modern climate change: current and anticipated future conditions in the western United States, Reviews of Geophysics, 58, e2019RG000692, https://doi.org/10.1029/2019RG000692, 2020.

Estermann, R., Rajczak, J., Velasquez, P., Lorenz, R. & Schär, C.: Projections of heavy precipitation characteristics over the Greater Alpine Region using a kilometer-scale climate model ensemble, Journal of Geophysical Research, 130, e2024JD040901, https://doi.org/10.1029/2024JD040901, 2025.

Fischer, K.: Die Murkegel des Vinschgaues, Der Schlern, 40(1), 24–34, 1965.

Fischer, J. & Stängl, O.: Das Hochwasser im Bayerischen Donaugebiet im Mai-Juni 1940, Landesstelle für Gewässerkunde, München, 1941.

Franke, D., Hornung, J. & Hinderer, M.: A combined study of radar facies, lithofacies and three-dimensional architecture of an alpine alluvial fan (Illgraben fan, Switzerland), Sedimentology, 62, 57–86, https://doi.org/10.1111/sed.12139, 2015.

Friedel., H.: Beobachtungen an den Schutthalden der Karawanken, Carinthia 125, 21–33, 1935.

Geosphere Austria: Stationsdaten, https://data.hub.geosphere.at/group/stationsdaten, last access 16 October 2025.

https://doi.org/10.5194/egusphere-2026-1699
Preprint. Discussion started: 13 April 2026

Gerig, G.: Bericht über die Unwetterkatastrophen vom 31. Juli und 1. August 1977 im Kanton Uri, Schweizerische Zeitschrift für Forstwesen, 128, 963–968, https://doi.org/10.5169/seals-766863, 1977.

Giorgi, F., Torma, C., Coppola, E., Ban, N., Schär, C. & Somot, S.: Enhanced summer convective rainfall at Alpine high elevations in response to climate warming, Nature Geoscience, https://doi.org/10.1038/NGEO2761, 2016.

GKD: Gewässerkundlicher Dienst Bayern, https://www.gkd.bayern.de/, last access: 16 October 2025.

Gobiet, A., Kotlarski, S., Beniston, M., Heinrich, G., Rajczak, J. & Stoffel, M.: 21st century climate change in the European Alps – a review, Science of the Total Environment, 493, 1138–1151, https://doi.org/10.1016/j.scitotenv.2013.07.050, 2014.

Godina, R., Lalk, P. Lorenz, P., Müller, G. & Weilguni, V.: Hochwasser 2005 Ereignisdokumentation. Teilbericht des Hydrographischen Dienstes, Bundesministerium für Land- und Forstwirtschaft, Umwelt und Wasserwirtschaft, Wien, 26 pp., 2006.

Götz, J. & Schrott, L.: Holocene sediment cascades in the German Alps, in: Landscapes and Landforms of Germany, edited by: Lehmkuhl, F., Böse, M. & Krautblatter, M., Springer, Cham, 475–491, https://doi.org/10.1007/978-3-031-77876-6_28, 2025.

Guzetti, F., Peruccacci, S., Rossi, M. & Stark, C.: The rainfall intensity-duration control of shallow landslides and debris flows: an update, Landslides, 5, 3–17, https://doi.org/10.1007/s10346-007-0112-1, 2008.

Gruber, P.: Unwetterschäden im Kanton St. Gallen, Schweizerische Zeitschrift für Forstwesen, 128, 973–975, https://doi.org/10.5168/seals-766865

GWKD: Statistik Garmisch o.d. Partnachmündung/Loisach, https://files.gkd.bayern.de/pegel_jahrbuchseiten/Jahrbuchseiten_Q_16401006_2021_Garmisch_oh_Partnach.pdf, last access: 16 October 2025, 2021.

Gringarten, E. & Deutsch, C.V.: Teacher's Aide Variogram Interpretation and Modeling, Mathematical Geology, 33, 508–534, https://doi.org/10.1023/A:1011093014141, 2001.

Harris, C.R., Millman, K.J., van der Walt, S.J., Gommers, R., Virtanen, P., Cournapeau, D., Wieser, E., Taylor, J., Berg, S., Smith, N.J., Kern, R., Picus, M., Hoyer, S., van Kerkwijk, M.H., Brett, M., Haldane, A., del Río, J.F., Wiebe, M., Peterson, P., Gérard-Marchant, P., Shappard, K., Reddy, T., Wekcesser, W., Abbasi, H., Gohlke, C. & Oliphant, T.E.: Array programming with NumPy, Nature, 585: 357–362, https://doi.org/10.1038/s41586-020-2649-2, 2020.

Harvey, A.M.: Geomorphic effects of a 100 year storm in the Howgill Fells, Northwest England, Zeitschrift für Geomorphologie, 30, 71–91, 1986.

Harvey, A.M.: Differential recovery from the effects of a 100-year storm: significance of long-term hillslope-channel coupling; Howgill Fells, northwest England, Geomorphology, 84, 192–208, https://doi.org/10.1016/j.geomorph.2006.03.009, 2007.

Harvey, A.M.: Local buffers to the sediment cascade: debris cones and alluvial fans, in: Sediment cascades: an integrated approach, edited by: Burt, T.P. & Allison, R.J., 153–180, https://doi.org/10.1002/9780470682876.ch6, 2010.

https://doi.org/10.5194/egusphere-2026-1699
Preprint. Discussion started: 13 April 2026

Harvey, A.M.: The coupling status of alluvial fans and debris cones: a review and synthesis, Earth Surface Processes and Landforms, 37, 64–76, https://doi.org/10.1002/esp.2213, 2011.

Hayashi, M.: Alpine Hydrogeology: The critical role of groundwater in sourcing the headwaters of the world, Groundwater, 58,498-510, https://doi.org/10.1111/gwat.12965, 2020.

Herron, N., & Wilson, C.: A water balance approach to assessing the hydrologic buffering potential of an alluvial fan, Water Resources Research, 37(2), 341-351, https://doi.org/10.1029/2000WR900253, 2001.

Hirschberg, J., Fatichi, S., Bennett, G.L., McArdell, B.W., Peleg, N., Lane, S.N., Schlunegger, F. & Molnar, P.: Climate change impacts on sediment yield and debris-flow activity in an Alpine catchment, Journal of Geophysical Research: Earth Surface, 126, e2020JF005739, https://doi.org/10.1029/2020JF005739, 2021.

Hock, R., Rasul, G., Adler, C., Cáceres, B., Gruber, S., Hirabayashi, Y., Jackson, M., Kääb, A., Kang, S., Kutuzov, S., Milner, A., Molau, U., Morin, S., Orlove, B. & Steltzer, H.: High Mountain Areas, in: IPCC Special Report on the Ocean and Cryosphere in a Changing Climate, edited by: Pörtner, H.-O., Roberts, D.C., Masson-Delmotte, V., Zhai, P., Tignor, M., Poloczanska, E., Mintenbeck, K. Alegría, A., Nicolai, M., Okem, A., Petzold, J., Rama, B. & Weyer, N.M., Cambridge/New York, 131–202, https://doi.org/10.1017/9781009157964.004, 2019.

Hydrographischer Dienst Österreich: Hydrographisches Jahrbuch von Österreich 1965, Band 73, Bundesministerium für Land- und Forstwirtschaft, Wien, 302 pp., 1970.

Hydrographischer Dienst Österreich: Hydrographisches Jahrbuch von Österreich 1977, Band 85, Bundesministerium für Land- und Forstwirtschaft, Wien, 1981.

Hydrographischer Dienst Österreich: Hydrographisches Jahrbuch von Österreich 1979, Band 87, Bundesministerium für Land- und Forstwirtschaft, Wien, 1982.

Hydrographischer Dienst Österreich: Hydrographisches Jahrbuch von Österreich 1981, Band 89, Bundesministerium für Land- und Forstwirtschaft, Wien, 1984.

James, M.R & Robson, S.: Mitigating systematic error in topographic models derived from UAV and ground-based image networks, Earth Surface Processes and Landforms, 39, 1413–1420, https://doi.org/10.1002/esp.3609, 2014.

Jomelli, V., Brunstein, D., Grancher, D. & Pech, P.: Is the response of hill slope debris flows to recent climate change unequivocal? A case study in the Massif des Ecrins (French Alps), Climatic Change, 85, 119–137, https://doi.org/10.1007/s10584-006-9209-0, 2007.

Kälin, W.: Unwetterschäden im Kanton Schwyz vom 31.7./1.8.77, Schweizerische Zeitschrift für Forstwesen, 128, 969–972, https://doi.org/10.5169/seals-766864, 1977.

Kaitna, R., Prenner, D., Switanek, M., Maraun, D., Stoffel, M. & Hrachowitz, M.: Changes of hydro-meteorological trigger conditions for debris flows in a future alpine climate, Science of the Total Environment, 872, 162227, https://doi.org/10.1016/j.scitotenv.2023.162227, 2023.

Kaitna, R., Schneuwly-Bollschweiler, M., Sausgruber, T., Moser, M., Stoffel, M. & Rudolf-Miklau, F.: Susceptibility and triggers for debris flows: emergence, loading, release and entrainment, in: Dating torrential processes on fans and cones,

https://doi.org/10.5194/egusphere-2026-1699
Preprint. Discussion started: 13 April 2026

edited by: Schneuwly-Bollschweiler, M., Stoffel, M. & Rudolf-Miklau, F., Springer, Dordrecht, 33–49, https://doi.org/10.1007/10.1007/978-94-007-4336-6_3, 2013.

Kern, H. & Streil, J.: Das Hochwasser im bayerischen Donaugebiet im Juni 1965, Besondere Mitteilung zum Deutschen Gewässerkundlichen Jahrbuch, 32, 1972.

Kido, R., Inoue, T., Hatono, M. & Yamanoi, K.: Assessing the impact of climate change on sediment discharge using a large ensemble rainfall dataset in Pekerebetsu River basin, Hokkaido, Progress in Earth and Planetary Science, 10, 54, https://doi.org/10.1016/10.1186/s40645-023-0058-0, 2023.

Kiefer, C.*, Oswald, P.*, Moernaut, J., Fabbri, S.C., Mayr, C., Strasser, M. & Krautblatter, M.: A 4000-year debris flow record based on amphibious investigations of fan delta activity in Plansee (Austria, Eastern Alps), Earth Surface Dynamics, 9, 1481–1503. DOI: 10.5194/esurf-9-1481-2021, 2021.

Koegel, L.: Beobachtungen an Schuttkegeln aus den Ammergauer Bergen, Mitteilungen der Geographischen Gesellschaft in München, 14, 97–118, 1920.

Kortenhaus, W.: Das Naturwaldreservat Friedergrieß, Jahrbuch des Vereins zum Schutz der Bergwelt, 52, 37–70, 1987.

Kotlarski, S., Gobiet, A., Morin, S., Olefs, M., Rajczak, J. & Samacoïts, Raphaëlle: 21st Century alpine climate change, Climate Dynamics, 60, 65–86, https://doi.org/10.1016/10.1007s00382-022-06303-3, 2023.

Ku, H.H.: Notes on the use of propagation of error formulas, Journal of Research of the National Bureau of Standards – C: Engineering and Instrumentation, 70, 263–273, 1966.

Lana-Renault, N., Alvera, B. & García-Ruiz, J.M.: Runoff and sediment transport during the snowmelt period in a Mediterranean high-mountain catchment, Arctic, Antarctic and Alpine Research, 43, 213–222, https://doi.org/10.1657/1938-4246-43.2.213, 2011.

Land Tirol: Laserscan Download Tirol, https://tiris.maps.arcgis.com/apps/webappviewer/index.html?id=5e3071044cb44e76843d110baef8b138, last access: 26 - September 2025.

Landesamt für Wasserwirtschaft: Hochwasser Mai 1999 gewässerkundliche Beschreibung, Bayerisches Landesamt für Wasserwirtschaft, München, 42 pp., 2003.

Lane, S.N. & Richards, K.S. (1996): Linking river channel form and process: time, space and causality revisited, Earth Surface Processes and Landforms, 22, 249–260, https://doi.org/10.1002/(SICI)1096-9837(199703)22:3<249::AID-ESP752>3.0.CO;2-7, 1996.

LDBV: Topographisches Archiv des Bayerischen Landesvermessungsamtes, Urpositionsblatt 878 Eibsee, Bayerisches Landesamt für Digitalisierung, Breitband und Vermessung, München, 1826.

LDBV: Topographisches Archiv des Bayerischen Landesvermessungsamtes, Topographischer Atlas vom Königreich Bayern 1 : 50 000 Blatt 97 Mittenwald, Bayerisches Landesamt für Digitalisierung, Breitband und Vermessung, München, 1835.

https://doi.org/10.5194/egusphere-2026-1699
Preprint. Discussion started: 13 April 2026

LDBV: Topographisches Archiv des Bayerischen Landesvermessungsamtes, Topographischer Atlas vom Königreich Bayern 1 : 50 000 Blatt 97 Mittenwald (West) , Bayerisches Landesamt für Digitalisierung, Breitband und Vermessung, München, 1880.

LDBV: Topographisches Archiv des Bayerischen Landesvermessungsamtes, Karte des Deutschen Reiches Blatt 672 Mittenwald, Bayerisches Landesamt für Digitalisierung, Breitband und Vermessung, München, 1912.

LDBV: Topographisches Archiv des Bayerischen Landesvermessungsamtes, Karte des Deutschen Reiches Blatt 672 Mittenwald, Bayerisches Landesamt für Digitalisierung, Breitband und Vermessung, München, 1923.

LDBV: Opendata Bayern, https://geodaten.bayern.de/opengeodata/, last access: 26 September 2025.

Legarda Garzon, L.F., Johnson, M.F., Mount, N. & Gomez, H.: Exploring the effects of catchment morphometry on overland flow response to extreme rainfall using a 2D hydraulic-hydrological model (IBER), Journal of Hydrology, 627, 130405, https://doi.org/10.1016/j.jhydrol.2023.130405, 2023.

LfU: Gewässerkundlicher Bericht Hochwasser 2005, Bayerisches Landesamt für Umwelt, Augsburg, 75 pp., 2007.

LfU: Das Bayerische Klimaprojektionsensemble. Audit und Ensemblebildung, Bayerisches Landesamt für Umwelt, Augsburg, 52 pp., 2020.

LfU: Hochwasser Mai/Juni 2024. Wasserwirtschaftlicher Bericht, Bayerisches Landesamt für Umwelt, Augsburg, 149 pp., 2025.

Liebscher, H.-J.: Abfluß, in: Lehrbuch der Hydrologie, Band 1: Allgemeine Hydrologie, 2nd edition, edited by: Baumgartner, A. & Liebscher, H.-J., Gebrüder Bornträger, Berlin/Stuttgart, 474–553. 2. Auflage, Berlin/Stuttgart, ISBN: 3443300022, 1996.

Milan, D.J. & Schwendel, A.C.: Climate-change driven increased flood magnitudes and frequency in the British uplands: geomorphologically informed scientific underpinning for upland flood-risk management, Earth Surface Processes and Landforms, 46, 3026–3044, https://doi.org/10.1002/esp.5206, 2021.

Milan, D.J.: Geomorphic impact and system recovery following an extreme flood in an upland stream: Thinhope Burn, northern England, UK, Geomorphology, 138, 319–328, https://doi.org/10.1016/j.geomorph.2011.09.017, 2012.

Milan, D.J.: Modelling differential geomorphic effectiveness in neighbouring upland catchments: implications for sediment and flood risk management in a wetter world, Progress in Physical Geography, 46, 124–151, https://doi.org/10.1177/03091333211045514, 2021.

Morche, D., Katterfeld, C., Fuchs, S. & Schmidt, K.-H.: The life-span of a small high mountain lake, the Vordere Blaue Gumpe in the Bavarian Alps, in: Sediment Dynamics and the Hydromorphology of Fluvial Systems, Dundee, UK, July 2006, IAHS Publication 306, 72–81, 2006.

Morche, D., Schmidt, K.-H., Heckmann, T. & Haas, F.: Hydrology and geomorphic effects of a high-magnitude flood in an Alpine river, Geografiska Annaler, 89 A (1), 5–19., 2007.

Morche, D. & Schmidt, K.-H.: Sediment transport in an alpine river before and after a dambreak flood event, Earth Surface Processes and Landforms, 37, 347–353, https://doi.org/10.1002/esp.2263, 2011.

https://doi.org/10.5194/egusphere-2026-1699
Preprint. Discussion started: 13 April 2026

Oss Cazzador, D., Rainaot, R., Mao, L., Martini, L. & Picco, L.: Coarse sediment transfer and geomorphic changes in an alpine headwater stream, Geomorphology, 376, 107569, https://doi.org/10.1016/j.geomorph.2020.107569, 2021.

Over, J.-S.R., Ritchie, A.C., Kranenburg, C.J., Brown, J.A., Buscombe, D.D., Noble, T., Sherwood, C.R., Warrick, J.A. & Wernette, P.A.: Processing Coastal Imagery with Agisoft Metashape Professional Edition, Version 1.6 – Structure from Motion workflow documentation, U.S. Geological Survey, 46 pp., Open File Report 2021-1039, 2021.

Pellegrini, G., Picco, L. & Rainato, R.: Integrated bedload monitoring for mobility threshold analysis in an alpine stream, in: Proceedings of the International Mid-Term Conference 2024 of AIIA, Padova, Italy, 17–19 June 2024, 58–65, https://doi.org/10.1007/978-3-031-84212-2_ 9, 2024.

Phillips, J.D. & van Dyke, C.: Principles of geomorphic disturbance and recovery in response to storms, Earth Surface Processes and landforms, 41, 971–979, https://doi.org/10.1002/esp.3912, 2016.

Praskievicz, S.: A coupled hierarchical modeling approach to simulating the geomorphic response of river systems to anthropogenic climate change, Earth Surface Processes and Landforms, 40, 1616–1630, https://doi.org/10.1002/esp.3740, 2015.

Rainato, R., Picco, L., Cavalli, M., Mao, L, Neveman, A.J. & Tarolli, P. (2018a): Coupling climate conditions, sediment sources and sediment transport in an Alpine basin, Land Degradataion and Development, 29, 1154–1166, https://doi.org/10.1102/ldr.2813, 2018a.

Rainato, R., Picco, L., Oss Cazzador, D. & Mao, L.: Bedload transport in a steep alpine stream: assessment of sediment mobility and virtual velocity using the bedload tracking, E3S Web of Conferences, 40,02027, https://doi.org/10.1051/e3sconf/20184002027, 2018b.

Rainato, R., Pellegrini, G., Lenzi, M.A. & Picco, L.: Interaction between climatic conditions, water- and sediment-fluxes in an alpine basin: long-term monthly and seasonal analysis, Geomorphology, 472, 109590, https://doi.org/10.1016/j.geomorph.2024.109590, 2025.

Rajczak, J., Pall, P. & Schär, C.: Projections of extreme precipitation events in regional climate simulations for Europe and the Alpine Region, Journal of Geophysical Research: Atmospheres, 118, 3610–3626, https://doi.org/10.1002/jgrd.50297, 2013.

Rickenmann, D. & Koschni, A.: Sediment loads due to fluvial transport and debris flows during the 2005 flood events in Switzerland, Hydrological Processes, 24, 993–1007, https://doi.org/10.1002/hyp.7536, 2010.

Rolstad, C., Haug, T. & Denby, B.: Spatially integrated geodetic glacier mass balance and its uncertainty based on geostatistical analysis: application to the western Svartisen ice cap, Norway, Journal of Glaciology, 55, 666–680, https://doi.org/10.3189/002214309789470950, 2009.

Sass, O.: Spatial patterns of rockfall intensity in the Northern Alps, Zeitschrift für Geomorphologie, Supplementband 138, 51–65, 2005.

https://doi.org/10.5194/egusphere-2026-1699
Preprint. Discussion started: 13 April 2026

Schmidt, L.K., Francke, T., Rottler, E., Blume, T., Schöber, J. & Bronstert, A.: Suspended sediment and discharge dynamics in a glaciated alpine environment: identifying crucial areas and time periods on several spatial and temporal scales in the Ötztal, Austria, Earth Surface Dynamics, 10, 653–669, https://doi.org/10.5194/esurf-10-653-2022, 2022.

Schweizerische Meteorologische Anstalt (1979): Annalen der Schweizerischen Meteorologischen Anstalt 1979. Schweizerische Meteorologische Anstalt, 310 pp., ISSN 0080-7338, 1979.

Scott, P.F. & Erskine, W.D.: Geomorphic effects of a large flood on fluvial fans, Earth Surface Processes and Landforms, 19, 95–108, https://doi.org/10.1002/esp.3290190202, 1994.

Stahl, N. & Hofstätter, M.: Vb-Zugbahnen und deren Auftreten als Serie mit Bezug zu den resultierenden Hochwassern in Bayern und Auswirkungen auf Rückhalteräume im Isareinzugsgebiet, Hydrologie & Wasserbewirtschaftung, 62, 77–97, https://doi.org/10.5675/HyWa_2018,2_2, 2018.

Stoffel, M., Tiranti, D. & Huggel, C.: Climate change impacts on mass movements – Case studies from the European Alps, Science of the Total Environment, 493, 1255–1266, https://doi.org/10.1016/j.scitotenv.2014.02.102, 2014.

Turkington, T., Remaître, A., Ettema, J., Hussin, H. & van Westen, C.: Assessing debris flow activity in a changing climate, Climatic change, 137, 293–305, https://doi.org/10.1007/s10584-016-1657-6, 2016.

Van Hamel, A., Molnar, P., Janzing, J. & Brunner, M.I.: Suspended sediment concentrations in Alpine rivers: from annual regimes to sub-daily extreme events, Hydrology and Earth System Sciences, 29, 2975–2995, https://doi.org/10.5194/hess-29-2975-2025, 2025.

Vermeesch, P. (2017): Error Propagation, in: Isotope Geology. Part I: Radiometric Geochronology, 63–68 https://doi.org/10.31223/osf.io/sj4ft, 2017.

Virtanen, P., Gommers, R., Oliphant, T.E., Haberland, M., Reddy, T., Cournapeau, D., Burovski, E., Peterson, P., Wekcesser, W., Bright, J., van der Walt, S.J., Brett, M., Wilson, J., Millman, K.J., Mayorov, N., Nelson, A.R.J., Jones, E., Kern, R., Larson, E., Carey, C.J., Polat, Í., Feng, Y., Moore, E.W., van der Plas, J., Laxalde, D., Perktold, J., Cimrman, R., Henriksen, I., Quintero, E.A., Harris, C.R., Archibald, A.M., Ribeiro, A.H., Pedregosa, F., van Mulbregt, P. & SciPy 1.0 Contributors (2020): SciPy 1.0: fundamental algorithms for scientific computing in Python, Nature Methods, 17, 261–272, https://doi.org/10.1038/s41586-020-2649-2, 2020.

Wagner, T.C. & Zehm, A.: Das Friedergries – Sukzessionskomplex eines alpinen Dolomit-Schwemmfächers. – Tuexenia Beiheft 14: 25–46., 2022.

Weber, M. & Braun, L.: Hochwasser aus den Alpen, Akademie Aktuell, 50, 59–65, 2014.

Wells, S.G. & Harvey, A.M.: Sedimentologic and geomorphic variations in storm-generated alluvial fans, Howgill Fells, northwest England, Geological Society of America Bulletin, 98, 182–198, 1987.

WMO: WMO guidelines on the calculation of climate normals, World Meteorological Organization, Geneva, 18 pp., ISBN: 978-92-63-11203-3, 2017.

https://doi.org/10.5194/egusphere-2026-1699
Preprint. Discussion started: 13 April 2026

Wöllner, R. & Wagner, T.C.: Saving species, time and money: application of unmanned aerial vehicles (UAVs) for monitoring of an endangered alpine river specialist in a small nature reserve, Biological Conservation, 233, 162–175, https://doi.org/10.1016/j.biocon.2019.02.037, 2018.

Zeller, J. & Röthlisberger, G.: Unwetterschäden in der Schweiz von 1972 bis 1981, Wasser, Energie, Luft, 75, 149–160., 1984.